Supporting Information

Dörfler et al. 10.1073/pnas.1212134110

SI Text

The supporting information is organized as follows.

In *SI Preliminaries and Notation*, we introduce some notation and recall some preliminaries.

SI Mathematical Models and Synchronization Notions provides a description of the considered coupled oscillator model, including a detailed modeling of a mechanical analog and a few power network models. Furthermore, we state our definition of synchronization and compare various synchronization conditions proposed for oscillator networks.

SI Mathematical Analysis of Synchronization provides a rigorous mathematical analysis of synchronization, which leads to the synchronization conditions proposed in the main text. Throughout our analysis, we provide various examples illustrating certain theoretical concepts and results, and we also compare our results with existing results in the synchronization and power network literature.

SI Robust Synchronization in Presence of Uncertainty extends our synchronization condition to the case where the network parameters can vary within prescribed upper and lower bounds. This parameter-varying approach can account for modeling uncertainties or unmodeled dynamics.

SI Statistical Synchronization Assessment provides a detailed account of our Monte Carlo simulation studies and the complex Kuramoto network studies. Throughout this section, we also recall the basics of probability estimation by Monte Carlo methods that allow us to establish a statistical synchronization result in a mathematically rigorous way.

Finally, the subsection on *Synchronization Assessment for Power Networks* describes the detailed simulation setup for the randomized Institute of Electrical and Electronics Engineers (IEEE) test systems, provides the simulation data used for the dynamic IEEE Reliability Test System 96 (RTS 96) power network simulations, illustrates a dynamic bifurcation scenario in the RTS 96 power network, and describes extensions of the results in the main text to variable load demands and load voltages.

SI Preliminaries and Notation

Vectors and Functions. Let $\mathbf{1}_n$ and $\mathbf{0}_n$ be the n-dimensional vector of unit and zero entries, and let $\mathbf{1}_n^\perp$ be the orthogonal complement of $\mathbf{1}_n$ in $\mathbb{R}^n$, that is, $\mathbf{1}_n^\perp \triangleq \{x \in \mathbb{R}^n : x \perp \mathbf{1}_n\}$. Let e_i^n be the ith canonical basis vector of $\mathbb{R}^n$, that is, the ith entry of e_i^n is 1 and all other entries are 0. Let $\mathbf{1}_{n\times n} = \mathbf{1}_n \cdot \mathbf{1}_n^T$ be the $(n\times n)$ matrix of unit entries. Given an n-tuple $(x_1,\ldots,x_n)$, let $x\in\mathbb{R}^n$ be the associated vector. For an ordered index set $\mathcal{I}$ of cardinality $|\mathcal{I}|$ and a 1D array $\{x_i\}_{i\in\mathcal{I}}$, we define $\mathrm{diag}(\{x_i\}_{i\in\mathcal{I}}) \in \mathbb{R}^{|\mathcal{I}|\times|\mathcal{I}|}$ to be the associated diagonal matrix. For $x\in\mathbb{R}^n$, we define the vector-valued functions $\mathbf{sin}(x) = (\sin(x_1),\ldots,\sin(x_n))$ and $\mathbf{arcsin}(x) = (\arcsin(x_1),\ldots,\arcsin(x_n))$, where the arcsin function is defined for the branch $[-\pi/2, \pi/2]$. For a set $\mathcal{X}\subset\mathbb{R}^n$ and a matrix $A\in\mathbb{R}^{m\times n}$, let $A\mathcal{X} = \{y\in\mathbb{R}^m : y = Ax,\ x\in\mathcal{X}\}$.

Geometry on *n*-Torus. The set $\mathbb{S}^1$ denotes the unit circle, an angle is a point $\theta\in\mathbb{S}^1$, and an arc is a connected subset of $\mathbb{S}^1$. The *geodesic distance* between two angles $\theta_1,\theta_2\in\mathbb{S}^1$ is the minimum of the counterclockwise and clockwise arc lengths connecting θ_1 and θ_2. With slight abuse of notation, let $|\theta_1-\theta_2|$ denote the *geodesic distance* between two angles $\theta_1,\theta_2\in\mathbb{S}^1$. Finally, the *n-torus*, the product set $\mathbb{T}^n = \mathbb{S}^1\times\cdots\times\mathbb{S}^1$, is the direct sum of n unit circles.

Algebraic Graph Theory. Given an undirected, connected, and weighted graph $G(\mathcal{V},\mathcal{E},A)$ induced by the symmetrical, irreducible, and nonnegative *adjacency matrix* $A\in\mathbb{R}^{n\times n}$, the Laplacian matrix $L\in\mathbb{R}^{n\times n}$ is defined by $L = \mathrm{diag}\big(\{\sum_{j=1}^n a_{ij}\}_{i=1}^n\big) - A$. If a number $\ell\in\{1,\ldots,|\mathcal{E}|\}$ and an arbitrary direction are assigned to each edge $\{i,j\}\in\mathcal{E}$, the (oriented) *incidence matrix* $B\in\mathbb{R}^{n\times|\mathcal{E}|}$ is defined component-wise as $B_{k\ell}=1$ if node k is the sink node of edge ℓ and as $B_{k\ell}=-1$ if node k is the source node of edge ℓ; all other elements are 0. For $x\in\mathbb{R}^n$, the vector B^Tx has components x_i-x_j for any oriented edge from j to i, that is, B^T maps node variables x_i and x_j to incremental edge variables x_i-x_j. If $\mathrm{diag}(\{a_{ij}\}_{\{i,j\}\in\mathcal{E}})$ is the diagonal matrix of nonzero edge weights, $L = B\ \mathrm{diag}(\{a_{ij}\}_{\{i,j\}\in\mathcal{E}})B^T$. For a vector $x\in\mathbb{R}^n$, the incremental norm $\|x\|_{\mathcal{E},\infty}\triangleq\max_{\{i,j\}\in\mathcal{E}}|x_i-x_j|$ used in the main text can be expressed via the incidence matrix B as $\|x\|_{\mathcal{E},\infty} = \|B^Tx\|_\infty$. If the graph is connected, $\mathrm{Ker}(B^T) = \mathrm{Ker}(L) = \mathrm{span}(\mathbf{1}_n)$, all $n-1$ remaining eigenvalues of L are real and strictly positive, and the second smallest eigenvalue $\lambda_2(L)$ is called the *algebraic connectivity*. The orthogonal vector spaces $\mathrm{Ker}(B)$ and $\mathrm{Ker}(B)^\perp = \mathrm{Im}(B^T)$ are spanned by vectors associated with cycles and cut-sets in the graph (e.g., ref. 1, section 4; ref. 2). In the following, we refer to $\mathrm{Ker}(B)$ and $\mathrm{Im}(B^T)$ as the *cycle space* and the *cut-set space*, respectively.

Laplacian Inverses. Because the Laplacian matrix L is singular, we will frequently use its *Moore–Penrose pseudo inverse* $L^\dagger$. If $U\in\mathbb{R}^{n\times n}$ is an orthonormal matrix of eigenvectors of L, the singular value decomposition of L is $L = U\ \mathrm{diag}(\{0,\lambda_2,\ldots,\lambda_n\})U^T$ and its Moore–Penrose pseudo inverse $L^\dagger$ is given by $L^\dagger = U\ \mathrm{diag}(\{0, 1/\lambda_2,\ldots,1/\lambda_n\})U^T$. We will frequently use the identity $L\cdot L^\dagger = L^\dagger\cdot L = I_n - \frac{1}{n}\mathbf{1}_{n\times n}$, which follows directly from the singular value decomposition. We also define the *effective resistance* between nodes i and j by $R_{ij} = L_{ii}^\dagger + L_{jj}^\dagger - 2L_{ij}^\dagger$. We refer to the study by Dörfler and Bullo (3) for further information on Laplacian inverses and on the resistance distance.

SI Mathematical Models and Synchronization Notions

In this section, we introduce the mathematical model of coupled phase oscillators considered in this article, present some synchronization notions, and give a detailed account of the literature on synchronization of coupled phase oscillators.

General Coupled Oscillator Model. Consider a weighted, undirected, and connected graph $G(\mathcal{V},\mathcal{E},A)$ with n nodes $\mathcal{V}=\{1,\ldots,n\}$, partitioned node set $\mathcal{V}=\mathcal{V}_1\cup\mathcal{V}_2$, and edge set $\mathcal{E}$ induced by the adjacency matrix $A\in\mathbb{R}^{n\times n}$. We assume that the graph G has no self-loops $\{i,i\}$ (i.e., $a_{ii}=0$ for all $i\in\mathcal{V}$). Associated with this graph, consider the following model of $|\mathcal{V}_1|\geq 0$ second-order Newtonian and $|\mathcal{V}_2|\geq 0$ first-order kinematic phase oscillators:

$$\begin{aligned} M_i\ddot{\theta}_i + D_i\dot{\theta}_i &= \omega_i - \sum_{j=1}^n a_{ij}\sin(\theta_i-\theta_j),\ \ i\in\mathcal{V}_1 \\ D_i\dot{\theta}_i &= \omega_i - \sum_{j=1}^n a_{ij}\sin(\theta_i-\theta_j),\ \ i\in\mathcal{V}_2, \end{aligned} \qquad \textbf{[S1]}$$

where $\theta_i\in\mathbb{S}^1$ and $\dot{\theta}_i\in\mathbb{R}^1$ are the phase and frequency of oscillator $i\in\mathcal{V}$, $\omega_i\in\mathbb{R}^1$ and $D_i>0$ are the natural frequency and damping coefficient of oscillator $i\in\mathcal{V}$, and $M_i>0$ is the inertial constant of oscillator $i\in\mathcal{V}_1$. The coupled oscillator model **[S1]** evolves on $\mathbb{T}^n\times\mathbb{R}^{|\mathcal{V}_1|}$ and features an important symmetry, namely, the rotational invariance of the angular variable θ. The interesting dynamics of the coupled oscillator model **[S1]** arise from a competition between each oscillator's tendency to align with its natural frequency ω_i and the synchronization-enforcing coupling $a_{ij}\sin(\theta_i-\theta_j)$ with its neighbors.

As discussed in the main text, the coupled oscillator model [**S1**] unifies various models proposed in the literature. For example, for the parameters $\mathcal{V}_1 = \emptyset$ and $D_i = 1$ for all $i \in \mathcal{V}_2$, it reduces to the celebrated *Kuramoto model* (4, 5)

$$\dot{\theta}_i = \omega_i - \sum_{j=1}^{n} a_{ij} \sin(\theta_i - \theta_j), \quad i \in \{1, \ldots, n\}. \qquad \textbf{[S2]}$$

We refer to specific reviews (6–10) for various theoretical results on the Kuramoto model [**S2**] and further synchronization applications in natural sciences, technology, and social networks. Here, we present a detailed modeling of the spring oscillator network used as a mechanical analog in the main text and present a few power network models, which can be described by the coupled oscillator model [**S1**].

Mechanical Spring Network. Consider the spring network illustrated in Fig. S1 consisting of a group of n particles constrained to rotate around a circle with unit radius. For simplicity, we assume that the particles are allowed to move freely on the circle and exchange their order without collisions.

Each particle is characterized by its phase angle $\theta_i \in \mathbb{S}^1$ and frequency $\dot{\theta}_i \in \mathbb{R}$, and its inertial and damping coefficients are $M_i > 0$ and $D_i > 0$, respectively. The external forces and torques acting on each particle are (*i*) a viscous damping force $D_i \dot{\theta}_i$ opposing the direction of motion, (*ii*) a nonconservative force $\omega_i \in \mathbb{R}$ along the direction of motion depicting a preferred natural rotation frequency, and (*iii*) an elastic restoring torque between interacting particles i and j coupled by an ideal elastic spring with stiffness $a_{ij} > 0$ and zero rest length. The topology of the spring network is described by the weighted, undirected, and connected graph $G(\mathcal{V}, \mathcal{E}, A)$.

To compute the elastic torque between the particles, we parametrize the position of each particle i by the unit vector $p_i = [\cos(\theta_i), \sin(\theta_i)]^T \in \mathbb{S}^1 \subset \mathbb{R}^2$. The elastic Hookean energy stored in the springs is the function $E : \mathbb{T}^n \to \mathbb{R}$ given up to an additive constant by

$$\begin{aligned} E(\theta) &= \sum_{\{i,j\} \in \mathcal{E}} \frac{a_{ij}}{2} \| p_i - p_j \|_2^2 \\ &= \sum_{\{i,j\} \in \mathcal{E}} a_{ij} \left(1 - \cos(\theta_i)\cos(\theta_j) - \sin(\theta_i)\sin(\theta_j)\right) \\ &= \sum_{\{i,j\} \in \mathcal{E}} a_{ij} \left(1 - \cos(\theta_i - \theta_j)\right), \end{aligned}$$

where we used the trigonometric identity $\cos(\alpha - \beta) = \cos\alpha \, \cos\beta + \sin\alpha \, \sin\beta$ in the last equality. Hence, we obtain the restoring torque acting on particle i as

$$T_i(\theta) = -\frac{\partial}{\partial \theta_i} E(\theta) = -\sum_{j=1}^{n} a_{ij} \sin(\theta_i - \theta_j).$$

Therefore, the network of spring-interconnected particles depicted in Fig. S1 obeys the dynamics

$$M_i \ddot{\theta}_i + D_i \dot{\theta}_i = \omega_i - \sum_{j=1}^{n} a_{ij} \sin(\theta_i - \theta_j), \quad i \in \{1, \ldots, n\}. \qquad \textbf{[S3]}$$

In conclusion, the spring network in Fig. S1 is a mechanical analog of the coupled oscillator model [**S1**] with $\mathcal{V}_2 = \emptyset$.

Power Network Model. The coupled oscillator model [**S1**] also includes a variety of power network models. We briefly present different power network models compatible with the coupled oscillator model [**S1**] and refer to work by Sauer and Pai (ref. 11, chapter 7) for a detailed derivation from a higher order first-principle model.

Consider a connected power network with generators $\mathcal{V}_1$ and load buses $\mathcal{V}_2$. The network is described by the symmetrical nodal admittance matrix $Y \in \mathbb{C}^{n \times n}$ (augmented with the generator transient reactances). If the network is lossless and the voltage levels $|V_i|$ at all nodes $i \in \mathcal{V}_1 \cup \mathcal{V}_2$ are constant, the *maximum real-power transfer* between any two nodes $i, j \in \mathcal{V}_1 \cup \mathcal{V}_2$ is $a_{ij} = |V_i| \cdot |V_j| \cdot \Im(Y_{ij})$, where $\Im(Y_{ij})$ denotes the susceptance of the transmission line $\{i,j\} \in \mathcal{E}$. With this notation, the swing dynamics of generator i are given by

$$M_i \ddot{\theta}_i + D_i \dot{\theta}_i = P_{\mathrm{m},i} - \sum_{j=1}^{n} a_{ij} \sin(\theta_i - \theta_j), \quad i \in \mathcal{V}_1, \qquad \textbf{[S4]}$$

where $\theta_i \in \mathbb{S}^1$ and $\dot{\theta}_i \in \mathbb{R}^1$ are the generator rotor angle and frequency; $\theta_j \in \mathbb{S}^1$ for $j \in \mathcal{V}_2$ are the voltage phase angles at the load buses; and $P_{\mathrm{m},i} > 0$, $M_i > 0$, and $D_i > 0$ are the mechanical power input from the prime mover, the generator inertia constant, and the damping coefficient, respectively.

For the load buses $\mathcal{V}_2$, we consider the following three load models illustrated in Fig. S2.

1) *PV buses with frequency-dependent loads*: All load buses are PV *buses*, that is, the active power demand $P_{\mathrm{l},i}$ and the voltage magnitude $|V_i|$ are specified for each bus. The real power drawn by load i consists of a constant term $P_{\mathrm{l},i} > 0$ and a frequency-dependent term $D_i \dot{\theta}_i$ with $D_i > 0$, as illustrated in Fig. S2*A*. The resulting real-power balance equation is

$$D_i \dot{\theta}_i + P_{\mathrm{l},i} = -\sum_{j=1}^{n} a_{ij} \sin(\theta_i - \theta_j), \quad i \in \mathcal{V}_2. \qquad \textbf{[S5]}$$

   The dynamics [**S4** and **S5**] are known as the *structure-preserving power network model* (12) and equal the coupled oscillator model [**S1**] for $\omega_i = P_{\mathrm{m},i}$, $i \in \mathcal{V}_1$, and $\omega_i = -P_{\mathrm{l},i}$, $i \in \mathcal{V}_2$.
2) *PV buses with constant power loads*: All load buses are PV buses, each load features a constant real-power demand $P_{\mathrm{l},i} > 0$, and the load damping in [**S5**] is neglected, that is, $D_i = 0$ in [**S5**]. The corresponding circuit-theoretical model is shown in Fig. S2*B*. If the angular distances $|\theta_i(t) - \theta_j(t)| < \pi/2$ are bounded for each transmission line $\{i,j\} \in \mathcal{E}$ (this condition will be precisely established in the next section), the resulting differential-algebraic system has the same local stability properties as the dynamics [**S4** and **S5**]; see ref. 13. Hence, all our results also apply locally to the structure-preserving power network model [**S4** and **S5**] with zero load damping $D_i = 0$ for $i \in \mathcal{V}_2$.
3) *Constant current and constant admittance loads*: If each load $i \in \mathcal{V}_2$ is modeled as a constant current demand I_i and an (inductive) admittance $Y_{i,\mathrm{shunt}}$ to ground as illustrated in Fig. S2*C*, the linear current-balance equations are $I = YV$, where $I \in \mathbb{C}^n$ and $V \in \mathbb{C}^n$ are the vectors of nodal current injections and voltages. After elimination of the bus variables V_i, $i \in \mathcal{V}_2$, through Kron reduction [**S3**], the resulting dynamics assume the form [**S3**] known as the (lossless) *network-reduced power system model* (14, 15). We refer to the studies by Dörfler and Bullo (3) and Sauer and Pai (11) for a detailed derivation of the network-reduced model.

The above model [**S4** and **S5**] is valid for an AC grid with a synchronous generator and load models 1–3. We remark that synchronous motor loads also assume the form [**S4**] with $P_{\mathrm{m},i} < 0$ (16), and a first-principle modeling of a DC power source connected to an AC grid via a droop-controlled inverter also results in [**S5**] (further details are provided in ref. 17).

Remark 1 (Voltage Dynamics). *To conclude this modeling section, we want to state a word of caution regarding the load models.*

The PV load models [**S1** *and* **S2**] *assume constant voltage magnitudes* $|V_i|$ *at the loads. Under normal operating conditions, the assumption of constant voltage magnitudes is well justified because voltage magnitudes are controlled at the generators and the* *active power flow $a_{ij}\sin(\theta_i-\theta_j)=|V_i|\cdot|V_j|\cdot\Im(Y_{ij})\cdot\sin(\theta_i-\theta_j)$ between two nodes $i,j\in\mathcal{V}_1\cup\mathcal{V}_2$ is primarily governed by the angular difference $\theta_i-\theta_j$ and not by the voltage magnitudes $|V_i|,|V_j|$. The latter assumption is known as the "decoupling assumption" in the power systems community. Whereas the model in* [**S4** *and* **S5**] *is well-adopted for power systems stability studies, the assumption of constant load voltage magnitudes ceases to hold in a heavily stressed grid (near a bifurcation point), where additional dynamic phenomena can occur, such as voltage collapse at the loads* (18). *In short, the coupling weights a_{ij} are not necessarily constant.*

Likewise, if the shunt admittance loads in the load model [**S3**] *are not constant (e.g., constant power loads can be transformed to voltage-dependent shunt admittances), the Kron reduction process may be ill-posed or the admittance matrix of the network-reduced model depends on the load voltages. In the latter case, the coupling weights a_{ij} are again not constant but depend on the load voltages.*

To account explicitly for such unmodeled voltage dynamics affecting the coupling weights a_{ij}, we study the coupled oscillator model [**S1**] *with interval-valued parameters in SI Robust Synchronization in the Presence of Uncertainty.*

Synchronization Notions. The following subsets of the n-torus $\mathbb{T}^n$ are essential for the synchronization problem: For $\gamma\in[0,\pi/2[$, let $\overline{\Delta}_G(\gamma)\subset\mathbb{T}^n$ be the closed set of angle arrays $(\theta_1,\ldots,\theta_n)$ with the property $|\theta_i-\theta_j|\le\gamma$ for $\{i,j\}\in\mathcal{E}$. Also, let $\Delta_G(\gamma)$ be the interior of $\overline{\Delta}_G(\gamma)$.

Definition 1. *A solution $(\theta,\dot\theta):\mathbb{R}_{\ge0}\to(\mathbb{T}^n,\mathbb{R}^{|\mathcal{V}_1|})$ to the coupled oscillator model* [**S1**] *is said to be synchronized if $\theta_0\in\overline{\Delta}_G(\gamma)$ and there exists $\omega_{\text{sync}}\in\mathbb{R}^1$ such that $\theta(t)=\theta_0+\omega_{\text{sync}}\mathbf{1}_n t \pmod{2\pi}$ and $\dot\theta(t)=\omega_{\text{sync}}\mathbf{1}_{|\mathcal{V}_1|}$ for all $t\ge0$.*

In other words, here, synchronized trajectories have the properties of *frequency synchronization and phase cohesiveness*, that is, all oscillators rotate with the same synchronization frequency ω_{sync}, and all their phases belong to the set $\overline{\Delta}_G(\gamma)$. For a power network model [**S4** and **S5**], the notion of phase cohesiveness is equivalent to bounded flows $|a_{ij}\sin(\theta_i-\theta_j)|\le a_{ij}\sin(\gamma)$ for all transmission lines $\{i,j\}\in\mathcal{E}$.

For the coupled oscillator model [**S1**], the explicit synchronization frequency is given by $\omega_{\text{sync}}\triangleq\sum_{i=1}^n\omega_i/\sum_{i=1}^n D_i$ (a detailed derivation is provided in ref. 9). By transforming to a rotating frame with frequency ω_{sync} and by replacing ω_i by $\omega_i-D_i\omega_{\text{sync}}$, we obtain $\omega_{\text{sync}}=0$ (or, equivalently, $\omega\in\mathbf{1}_n^\perp$) corresponding to balanced power injections $\sum_{i\in\mathcal{V}_1}P_{\text{m},i}=\sum_{i\in\mathcal{V}_2}P_{\text{l},i}$ in power network applications. Hence, without loss of generality, we assume that $\omega\in\mathbf{1}_n^\perp$ such that $\omega_{\text{sync}}=0$.

Given a point $r\in\mathbb{S}^1$ and an angle $s\in[0,2\pi]$, let $\text{rot}_s(r)\in\mathbb{S}^1$ be the rotation of r counterclockwise by the angle s. For $(r_1,\ldots,r_n)\in\mathbb{T}^n$, define the equivalence class

$$[(r_1,\ldots,r_n)]=\{(\text{rot}_s(r_1),\ldots,\text{rot}_s(r_n))\in\mathbb{T}^n|s\in[0,2\pi]\}.$$

Clearly, if $(r_1,\ldots,r_n)\in\overline{\Delta}_G(\gamma)$, then $[(r_1,\ldots,r_n)]\subset\overline{\Delta}_G(\gamma)$.

Definition 2. *Given $\theta\in\overline{\Delta}_G(\gamma)$ for some $\gamma\in[0,\pi/2[$, the set $([\theta],\mathbf{0}_{|\mathcal{V}_1|})\subset\mathbb{T}^n\times\mathbb{R}^{|\mathcal{V}_1|}$ is a synchronization manifold of the coupled oscillator model* [**S1**].

Note that a synchronized solution takes value in a synchronization manifold due to rotational symmetry. For two first-order oscillators [**S2**], the state space $\mathbb{T}^2$, the set $\Delta_G(\pi/2)$, and the synchronization manifold $[\theta^*]$ associated with an angle array $\theta^*=(\theta_1^*,\theta_2^*)\in\mathbb{T}^2$ are illustrated in Fig. S3.

Existing Synchronization Conditions. The coupled oscillator dynamics [**S1**], and the Kuramoto dynamics [**S2**] for that matter, feature (*i*) the synchronizing effect of the coupling described by the weighted edges of the graph $G(\mathcal{V},\mathcal{E},A)$ and (*ii*) the desynchronizing effect of the dissimilar natural frequencies $\omega\in\mathbf{1}_n^\perp$ at the nodes. Loosely speaking, synchronization occurs when the coupling dominates the dissimilarity. Various conditions are proposed in the power systems and synchronization literature to quantify this tradeoff between coupling and dissimilarity. The coupling is typically quantified by the algebraic connectivity $\lambda_2(L)$ (15, 19–23) or by the weighted nodal degree $\text{deg}_i\triangleq\sum_{j=1}^n a_{ij}$ (3, 15, 24–26), and the dissimilarity is quantified by either absolute norms $\|\omega\|_p$ or incremental (relative) norms $\|B^T\omega\|_p$, where, typically, $p\in\{2,\infty\}$. Sometimes, these conditions can be evaluated only numerically because they are state-dependent (19, 24) or arise from a nontrivial linearization process, such as the Master stability function formalism (22, 23, 27). In general, concise and accurate results are only known for specific topologies, such as complete graphs (9, 28), linear chains (29, 30), and complete bipartite graphs (31) with uniform weights.

For arbitrary coupling topologies, only sufficient conditions are known (15, 19, 20, 24), as well as numerical investigations for random networks (21, 32–34). To best of our knowledge, the sharpest and provably correct synchronization conditions for arbitrary topologies assume the form $\lambda_2(L)>\left(\sum_{\{i,j\}\in\mathcal{E}}|\omega_i-\omega_j|^2\right)^{1/2}$ (ref. 10, theorem 4.7). For arbitrary undirected, connected, and weighted graphs $G(\mathcal{V},\mathcal{E},A)$, simulation studies indicate that the known sufficient conditions (15, 19, 20, 24) are conservative estimates on the threshold from incoherence to synchrony, and every review article on synchronization concludes with the open problem of finding sharp synchronization conditions (6, 7, 9, 22, 23, 35).

Mathematical Analysis of Synchronization

This section presents our analysis of the synchronization problem in the coupled oscillator model [**S1**].

Algebraic Approach to Synchronization. Here, we present a previously unexplored analysis approach that reduces the synchronization problem to an equivalent algebraic problem that reveals the crucial role of cycles and cut-sets in the graph topology. In a first analysis step, we reduce the synchronization problem for the coupled oscillator model [**S1**] to a simpler problem, namely, stability of a first-order model. It turns out that existence and local exponential stability of synchronized solutions of the coupled oscillator model [**S1**] can be entirely described by means of the first-order Kuramoto model [**S2**].

Lemma 1 (Synchronization Equivalence). *Consider the coupled oscillator model* [**S1**] *and the Kuramoto model* [**S2**]. *The following statements are equivalent for any $\gamma\in[0,\pi/2[$ and any synchronization manifold $([\theta],\mathbf{0}_{|\mathcal{V}_1|})\subset\overline{\Delta}_G(\gamma)\times\mathbb{R}^{|\mathcal{V}_1|}$:*

i) *$[\theta]$ is a locally exponentially stable synchronization manifold of the Kuramoto model* [**S2**].

ii) *$([\theta],\mathbf{0}_{|\mathcal{V}_1|})$ is a locally exponentially stable synchronization manifold of the coupled oscillator model* [**S1**].

If the equivalent statements (*i*) *and* (*ii*) *are true, then locally near their respective synchronization manifolds, the coupled oscillator model* [**S1**] *and the Kuramoto model* [**S2**], *together with the frequency dynamics $\frac{d}{dt}\dot\theta=-M^{-1}D\dot\theta$, are topologically conjugate.*

Loosely speaking, the topological conjugacy result means that the trajectories of the two plots in Fig. S4 can be continuously deformed to match each other while preserving parameterization of time. *Lemma 1* is illustrated in Fig. S4, and its proof can be found in the study by Dörfler and Bullo (ref. 9, theorems 5.1 and 5.3).

By *Lemma 1*, the local synchronization problem for the coupled oscillator model [**S1**] reduces to the synchronization problem for the first-order Kuramoto model [**S2**]. Henceforth, we restrict ourselves to the Kuramoto model [**S2**]. The following result is known in the synchronization literature (15, 20) as well as in power systems, where the saturation of a transmission line corresponds to a singularity of the load flow Jacobian, resulting in a saddle-node bifurcation (12, 13, 18, 19, 24, 36–42).

Lemma 2 (Stable Synchronization in ($\Delta_G\pi/2$)). *Consider the Kuramoto model* **[S2]** *with a connected graph* $G(\mathcal{V},\mathcal{E},A)$, *and let* $\gamma \in [0,\pi/2[$.

The following statements hold:

1) **Jacobian:** *The Jacobian of the Kuramoto model evaluated at* $\theta \in \mathbb{T}^n$ *is given by*

$$J(\theta) = -B\ \mathrm{diag}\Big(\big\{a_{ij}\cos(\theta_i - \theta_j)\big\}_{\{i,j\}\in\mathcal{E}}\Big)B^T.$$

2) **Stability:** *If there exists an equilibrium point* $\theta^* \in \overline{\Delta}_G(\gamma)$, *it belongs to a locally exponentially stable equilibrium manifold* $[\theta^*] \in \overline{\Delta}_G(\gamma)$.
3) **Uniqueness:** *This equilibrium manifold is unique in* $\overline{\Delta}_G(\pi/2)$.

Proof: Because we have that $\frac{\partial}{\partial\theta_i}(\omega_i - \sum_{k=1}^n a_{ik}\sin(\theta_i-\theta_k)) = -\sum_{k=1}^n a_{ik}\cos(\theta_i-\theta_k)$ and $\frac{\partial}{\partial\theta_j}(\omega_i - \sum_{k=1}^n a_{ik}\sin(\theta_i-\theta_k)) = a_{ij}\cos(\theta_i-\theta_j)$, the negative Jacobian of the right-hand side of the Kuramoto model **[S2]** equals the Laplacian matrix of the connected graph $G(\mathcal{V},\mathcal{E},\tilde{A})$, where $\tilde{a}_{ij} = a_{ij}\cos(\theta_i-\theta_j)$. Equivalently, in compact notation, the Jacobian is given by $J(\theta) = -B\,\mathrm{diag}(\{a_{ij}\cos(\theta_i-\theta_j)\}_{\{i,j\}\in\mathcal{E}})B^T$. This completes the proof of statement 1.

The Jacobian $J(\theta)$ evaluated at an equilibrium point $\theta^* \in \overline{\Delta}_G(\gamma)$ is negative semidefinite with rank $n-1$. Its nullspace is $\mathbf{1}_n$ and arises from the rotational symmetry of the right-hand side of the Kuramoto model **[S2]** (an illustration is provided in Fig. S3). Consequently, the equilibrium point $\theta^* \in \overline{\Delta}_G(\gamma)$ is locally (transversally) exponentially stable. Moreover, the corresponding equilibrium manifold $[\theta^*] \in \overline{\Delta}_G(\gamma)$ is locally exponentially stable. This completes the proof of statement 2.

To prove statement 3, we denote the right-hand side of **[S2]** by $f:\mathbb{T}^n \to \mathbb{R}^n$, where f is defined component-wise by

$$f_i(\theta) = \omega_i - \sum_{j=1}^n a_{ij}\sin(\theta_i-\theta_j),\ \ i\in\{1,\ldots,n\}.$$

In ref. 39 (corollary 1), it is shown that $f-\omega$ is a one-to-one function on $\overline{\Delta}_G(\pi/2)$ modulo rotational symmetry, that is, for $\theta_1 \in \overline{\Delta}_G(\pi/2)$ and $\theta_2 \in \overline{\Delta}_G(\pi/2)$, we have that $f(\theta_1) = f(\theta_2)$ if and only if $[\theta_1] = [\theta_2]$. This proves uniqueness of the equilibrium manifold in $\overline{\Delta}_G(\pi/2)$. ■

By *Lemma 2*, the problem of finding a locally stable synchronization manifold reduces to that of finding a fixed point $\theta^* \in \overline{\Delta}_G(\gamma)$ for some $\gamma \in [0,\pi/2[$. The fixed-point equations of the Kuramoto model **[S2]** read as follows:

$$\omega_i = \sum_{j=1}^n a_{ij}\sin(\theta_i-\theta_j),\ \ i\in\{1,\ldots,n\}. \qquad \textbf{[S6]}$$

In a compact notation, the fixed-point equations **[S6]** are

$$\omega = B\,\mathrm{diag}\Big(\big\{a_{ij}\big\}_{\{i,j\}\in\mathcal{E}}\Big)\mathbf{sin}(B^T\theta). \qquad \textbf{[S7]}$$

The following conditions show that the natural frequencies ω have to be absolutely and incrementally bounded and the nodal degree has to be sufficiently large such that fixed points of **[S6]** exist.

Lemma 3 (Necessary Synchronization Conditions). *Consider the Kuramoto model* **[S2]** *with graph* $G(\mathcal{V},\mathcal{E},A)$ and $\omega \in \mathbf{1}_n^\perp$. *Let* $\gamma\in[0,\pi/2[$, *and define the weighted nodal degree* $\deg_i \triangleq \sum_{j=1}^n a_{ij}$ *for each node* $i\in\{1,\ldots,n\}$.

The following statements hold:

1) **Absolute boundedness**: *If there exists a synchronized solution* $\theta\in\overline{\Delta}_G(\gamma)$,

$$\deg_i \sin(\gamma) \ge |\omega_i| \ \text{ for all } i\in\{1,\ldots,n\}. \qquad \textbf{[S8]}$$

2) **Incremental boundedness**: *If there exists a synchronized solution* $\theta\in\overline{\Delta}_G(\gamma)$,

$$\Big(\deg_i + \deg_j\Big)\sin(\gamma) \ge |\omega_i - \omega_j| \quad \text{for all } \{i,j\}\in\mathcal{E}. \qquad \textbf{[S9]}$$

Proof: The first condition arises because $\sin(\theta_i-\theta_j) \in [-\sin(\gamma),\sin(\gamma)]$ for $\theta\in\overline{\Delta}_G(\gamma)$, and the fixed-point equation **[S6]** has no solution if condition **[S8]** is not satisfied.

Alternatively, because $\omega\in\mathbf{1}_n^\perp$, multiplication of the fixed-point equation **[S7]** by the vector $(e_i^n - e_j^n)\in\mathbf{1}_n^\perp$ for $\{i,j\}\in\mathcal{E}$ or, equivalently, subtraction of the ith and jth fixed-point equation **[S6]** yields the following equation for all $\{i,j\}\in\mathcal{E}$:

$$\omega_i - \omega_j = \sum_{k=1}^n\big(a_{ik}\sin(\theta_i-\theta_k) - a_{jk}\sin(\theta_j-\theta_k)\big). \qquad \textbf{[S10]}$$

Again, **[S10]** has no solution in $\overline{\Delta}_G(\gamma)$ if condition **[S9]** is not satisfied. ■

In the following, we aim to find sufficient and sharp conditions under which the fixed-point equation **[S7]** admits a solution $\theta^*\in\overline{\Delta}_G(\gamma)$. We resort to a rather straightforward solution ansatz. By formally replacing each term $\sin(\theta_i-\theta_j)$ in the fixed-point equations **[S7]** by an auxiliary scalar variable ψ_{ij}, the fixed-point equation **[S7]** is equivalently written as

$$\omega = B\,\mathrm{diag}\Big(\big\{a_{ij}\big\}_{\{i,j\}\in\mathcal{E}}\Big)\psi, \qquad \textbf{[S11]}$$

$$\psi = \mathbf{sin}(B^T\theta), \qquad \textbf{[S12]}$$

where $\psi\in\mathbb{R}^{|\mathcal{E}|}$ is a vector with elements ψ_{ij}. We will refer to **[S11]** as the *auxiliary fixed-point equation* and characterize its properties in the following theorem.

Theorem 1 (Properties of the Fixed-Point Equations). *Consider the Kuramoto model* **[S2]** *with graph* $G(\mathcal{V},\mathcal{E},A)$ *and* $\omega\in\mathbf{1}_n^\perp$, its *fixed point equation* **[S7]**, *and the auxiliary fixed-point equation* **[S11]**.

The following statements hold:

1) **Exact solution:** *Every solution of the auxiliary fixed-point equation* **[S11]** *is of the form*

$$\psi = B^T L^\dagger \omega + \psi_{\mathrm{hom}}, \qquad \textbf{[S13]}$$

where the homogeneous solution $\psi_{\mathrm{hom}}\in\mathbb{R}^{|\mathcal{E}|}$ *satisfies* $\mathrm{diag}(\{a_{ij}\}_{\{i,j\}\in\mathcal{E}})\,\psi_{\mathrm{hom}}\in\mathrm{Ker}(B)$.
2) **Exact synchronization condition:** *Let* $\gamma\in[0,\pi/2[$. *The following three statements are equivalent:*
   (*i*) *There exists a solution* $\theta^*\in\overline{\Delta}_G(\gamma)$ *to the fixed-point equation* **[S7]**.
   (*ii*) *There exists a solution* $\theta\in\overline{\Delta}_G(\gamma)$ *to*

$$B^T L^\dagger\omega + \psi_{\mathrm{hom}} = \mathbf{sin}(B^T\theta) \qquad \textbf{[S14]}$$

   for some $\psi_{\mathrm{hom}}\in\mathrm{diag}(\{1/a_{ij}\}_{\{i,j\}\in\mathcal{E}})\mathrm{ker}(B)$.
   (*iii*) *There exists a solution* $\psi\in\mathbb{R}^{|\mathcal{E}|}$ *to the auxiliary fixed-point equation* **[S11]** *of the form* **[S13]** *satisfying the norm constraint* $\|\psi\|_\infty \le \sin(\gamma)$ *and the cycle constraint* $\mathbf{arcsin}(\psi)\in\mathrm{Im}(B^T)$.

If the three equivalent statements (*i*) *to* (*iii*) *are true, we have the identities* $B^T\theta^* = B^T\theta = \mathbf{arcsin}(\psi)$. *Additionally,* $[\theta^*] \in \overline{\Delta}_G(\gamma)$ *is a locally exponentially stable synchronization manifold*.

Proof: Statement 1. Every solution $\psi \in \mathbb{R}^{|\mathcal{E}|}$ to the auxiliary fixed-point equation [**S11**] is of the form $\psi = \psi_{\text{hom}} + \psi_{\text{pt}}$, where ψ_{hom} is the homogeneous solution and ψ_{pt} is a particular solution. The homogeneous solution satisfies $B\,\text{diag}(\{a_{ij}\}_{\{i,j\}\in\mathcal{E}})\psi_{\text{hom}} = \mathbf{0}_n$. One can easily verify that $\psi_{\text{pt}} = B^T L^\dagger \omega$ is a particular solution,[‡] because $B\,\text{diag}(\{a_{ij}\}_{\{i,j\}\in\mathcal{E}})\psi_{\text{pt}} = B\,\text{diag}(\{a_{ij}\}_{\{i,j\}\in\mathcal{E}})B^T L^\dagger \omega = LL^\dagger\omega = \left(I_n - \frac{1}{n}\mathbf{1}_{n\times n}\right)\,\omega = \omega$.

Statement 2. Equivalence $[(i)\Leftrightarrow(ii)]$**:**

If there exists a solution θ^* of the fixed-point equation [**S7**], θ^* can be equivalently obtained from [**S12**], together with the solution [**S13**] of the auxiliary equation [**S11**]. These two equations directly give [**S14**].

Equivalence $[(ii)\Leftrightarrow(iii)]$**:**

For $\theta^* \in \overline{\Delta}_G(\gamma)$, we have from [**S14**] that $\|\psi\|_\infty \le \sin(\gamma)$ and $\mathbf{arcsin}(\psi) = B^T\theta^*$, that is, $\mathbf{arcsin}(\psi) \in \text{Im}(B^T)$. Conversely, if the norm constraint $\|\psi\|_\infty \le \sin(\gamma)$ and the cycle constraint $\mathbf{arcsin}(\psi) \in \text{Im}(B^T)$ are met, [**S14**] is solvable in $\overline{\Delta}_G(\gamma)$, that is, there is $\theta^* \in \overline{\Delta}_G(\gamma)$ such that $\mathbf{arcsin}(\psi) = B^T\theta^*$. The local exponential stability of the associated synchronization manifold $[\theta^*]$ follows then directly from *Lemma 2*. ■

The particular solution $B^T L^\dagger \omega$ to the auxiliary fixed-point equation [**S11**] lives in the cut-set space $\text{Ker}(B)^\perp$, and the homogeneous solution ψ_{hom} lives in the weighted cycle space $\psi_{\text{hom}} \in \text{diag}(\{1/a_{ij}\}_{\{i,j\}\in\mathcal{E}})\text{Ker}(B)$. As a consequence, by statement (*iii*) of *Theorem 1*, for each cycle in the graph, we obtain one degree of freedom in choosing the homogeneous solution ψ_{hom} as well as one nonlinear constraint $c^T\mathbf{arcsin}(\psi) = 0$, where $c \in \ker(B)$ is a signed path vector corresponding to the cycle.

Remark 2 (Comments on Necessity). *The cycle space* $\text{Ker}(B)$ *of the graph serves as a degree of freedom to find a minimum* ∞*-norm solution* ψ^* *to* [**S11**] *via*

$$\min_{\psi\in\mathbb{R}^{|\mathcal{E}|}} \|\psi\|_\infty \text{subject to } \omega = B\,\text{diag}\left(\{a_{ij}\}_{\{i,j\}\in\mathcal{E}}\right)\psi. \qquad [\mathbf{S15}]$$

By Theorem 1, such a minimum ∞*-norm solution* ψ^* *necessarily satisfies* $\|\psi^*\|_\infty \le \sin(\gamma)$ *such that an equilibrium* $\theta^* \in \overline{\Delta}_G(\gamma)$ *exists. Hence, the condition* $\|\psi^*\|_\infty \le \sin(\gamma)$ *is an optimal necessary synchronization condition*.

The optimization problem [**S15**], *the minimum* ∞*-norm solution to an underdetermined and consistent system of linear equations, is well studied in the context of kinematically redundant manipulators. Its solution is known to be nonunique and contained in a disconnected solution space (43, 44). Unfortunately, there is no "a priori" analytical formula to construct a minimum* ∞*-norm solution, but the optimization problem is computationally tractable via its dual problem* $\max_{u\in\mathbb{R}^n} u^T\omega$ *subject to* $\|\text{diag}(\{a_{ij}\}_{\{i,j\}\in\mathcal{E}})B^T u\|_1 = 1$.

Synchronization Assessment for Specific Networks. In this section, we seek to establish that the condition

$$\left\|B^T L^\dagger \omega\right\|_\infty = \left\|L^\dagger\omega\right\|_{\mathcal{E},\infty} < 1 \qquad [\mathbf{S16}]$$

is sufficient for the existence of locally exponentially stable equilibria in $\Delta_G(\pi/2)$. More generally, for a given level of phase cohesiveness $\gamma \in [0, \pi/2[$, we seek to establish that the condition

$$\left\|B^T L^\dagger \omega\right\|_\infty = \left\|L^\dagger\omega\right\|_{\mathcal{E},\infty} \le \sin(\gamma) \qquad [\mathbf{S17}]$$

is sufficient for the existence of locally exponentially stable equilibria in $\overline{\Delta}_G(\gamma)$. Because the right-hand side of [**S17**] is a concave function of $\gamma \in [0, \pi/2[$ that achieves its supremum value at $\gamma^* = \pi/2$, it follows that condition [**S17**] implies [**S16**].

In the main text, we provide a detailed interpretation of the synchronization conditions [**S16** and **S17**] from various practical perspectives. Before continuing our theoretical analysis, we provide two further abstract but insightful perspectives on the conditions [**S16** and **S17**].

Remark 3 (Interpretation of the Synchronization Condition). ***Graph-theoretical interpretation.*** *With regard to the exact and state-dependent norm and cycle conditions in statement* (*iii*) *of Theorem 1, the proposed condition* [**S17**] *is simply a norm constraint on the network parameters in cut-set space* $\text{Im}(B^T)$ *of the graph topology, and cycle components are discarded*.

Circuit-theoretical interpretation. *In a circuit or power network, the variable* $\omega \in \mathbb{R}^n$ *corresponds to nodal power injections. Let* $x \in \mathbb{R}^{|\mathcal{E}|}$ *satisfy* $Bx = \omega$; *x then corresponds to equivalent power injections along lines* $\{i,j\} \in \mathcal{E}$.[§] *Condition* [**S16**] *can then be rewritten as* $\|B^T L^\dagger Bx\|_\infty < 1$. *The matrix* $B^T L^\dagger B \in \mathbb{R}^{|\mathcal{E}|\times|\mathcal{E}|}$ *has elements* $(e_n^i - e_n^j)^T L^\dagger (e_n^k - e_n^\ell)$ for $\{i,j\},\{k,\ell\} \in \mathcal{E}$, *its diagonal elements are the effective resistances* R_{ij}, *and its off-diagonal elements are the network distribution (sensitivity) factors (ref. 45, appendix 11A). Hence, from a circuit-theoretical perspective, condition* [**S16**] *restricts the pairwise effective resistances and the routing of power through the network similar to the resistive synchronization conditions developed elsewhere (3, 24, 25)*.

As it turns out, the exact state-dependent synchronization conditions in *Theorem 1* can be easily evaluated for the sparsest (acyclic) and densest (homogeneous) topologies and for "worst-case" (cut-set inducing) and "best-case" (identical) natural frequencies. For all these cases, the scalar condition [**S17**] is sharp. To quantify a "sharp" condition in the following theorem, we distinguish between *exact* (necessary and sufficient) conditions and *tight* conditions, which are sufficient in general and become necessary over a set of parametric realizations.

Theorem 2 (Synchronization Condition for Extremal Network Topologies and Parameters). *Consider the Kuramoto model* [**S2**] *with connected graph* $G(\mathcal{V},\mathcal{E},A)$ *and* $\omega \in \mathbf{1}_n^\perp$. *Consider the inequality condition* [**S17**] *for* $\gamma \in [0, \pi/2[$.

The following statements hold:

G1) **Exact synchronization condition for acyclic graphs:** *Assume that* $G(\mathcal{V},\mathcal{E},A)$ *is acyclic. There exists a locally exponentially stable equilibrium* $\theta^* \in \overline{\Delta}_G(\gamma)$ *if and only if condition* [**S17**] *holds. Moreover, in this case, we have that* $B^T\theta^* = \mathbf{arcsin}(B^T L^\dagger\omega) \in \overline{\Delta}_G(\gamma)$.

G2) **Tight synchronization condition for homogeneous graphs:** *Assume that* $G(\mathcal{V},\mathcal{E},A)$ *is a homogeneous graph, that is, there is* $K > 0$ *such that* $a_{ij} = K$ *for all distinct* $i,j \in \{1,\ldots,n\}$. *Consider a compact interval* $\Omega \subset \mathbb{R}$, *and let* $\mathbf{\Omega} = (\mathbf{\Omega}_1,\ldots,\mathbf{\Omega}_n) \subset \mathbb{R}^n$ *be the set of all vectors with components* $\mathbf{\Omega}_i \in \Omega$ *for all* $i \in \{1,\ldots,n\}$. *For all* $\omega \in \mathbf{\Omega}$, *there exists a locally exponentially stable equilibrium* $\theta^* \in \overline{\Delta}_G(\gamma)$ *if and only if condition* [**S17**] holds.

G3) **Exact synchronization condition for cut-set inducing natural frequencies:** *Let* $\Omega_1, \Omega_2 \in \mathbb{R}$, *and let* $\mathbf{\Omega} = (\mathbf{\Omega}_1,\ldots,\mathbf{\Omega}_n) \subset \mathbb{R}^n$

[‡]Likewise, it can also be shown that $(B\,\text{diag}(\{a_{ij}\}_{\{i,j\}\in\mathcal{E}}))^\dagger\omega$ and $\text{diag}(\{a_{ij}\}_{\{i,j\}\in\mathcal{E}})^{-1}B^\dagger\omega$ are other possible particular solutions. All these solutions differ only by the addition of a homogeneous solution. Each one can be interpreted as the solution to a weighted least-squares problem (43). Further solutions can also be constructed in a graph-theoretical way by spanning-tree decomposition (2). Our specific choice $\psi_{\text{pt}} = B^T L^\dagger\omega$ has the property that $\psi_{\text{pt}} \in \text{Im}(B^T)$ lives in the cut-set space, and it is the most useful particular solution with which to proceed with our synchronization analysis.

[§]Notice that *x* is not uniquely determined if the circuit features loops.

be the set of bipolar vectors with components $\boldsymbol{\Omega}_i \in \{\Omega_1, \Omega_2\}$ *for* $i \in \{1, \ldots, n\}$. *For all* $\omega \in L\boldsymbol{\Omega}$, *there exists a locally exponentially stable equilibrium* $\theta^* \in \overline{\Delta}_G(\gamma)$ *if and only if condition* **[S17]** *holds. Moreover,* $\boldsymbol{\Omega}$ *induces a cut-set: If* $|\Omega_2 - \Omega_1| = \sin(\gamma)$, *for any particular* $\boldsymbol{\Omega}^* \in \boldsymbol{\Omega}$ *and* $\omega = L\boldsymbol{\Omega}^*$, *we obtain the equilibrium* $\theta^* \in \overline{\Delta}_G(\gamma)$ *satisfying* $B^T\theta^* = \mathbf{arcsin}(B^T\boldsymbol{\Omega}^*)$, *that is, for all* $\{i,j\} \in \mathcal{E}$, $|\theta_i^* - \theta_j^*| = 0$ *if* $\boldsymbol{\Omega}_i^* = \boldsymbol{\Omega}_j^*$ *and* $|\theta_i^* - \theta_j^*| = \gamma$ if $\boldsymbol{\Omega}_i^* \neq \boldsymbol{\Omega}_j^*$.

G4) **Asymptotic correctness:** *In the limit* $\|B^TL^\dagger\omega\|_\infty \to 0$, *that is, for identical natural frequencies and/or asymptotically strong network coupling, there is a locally exponentially stable equilibrium* θ^* *satisfying*

$$\lim_{\|B^TL^\dagger\omega\|_\infty \to 0} \frac{(B^T\theta^*)_i}{(\mathbf{arcsin}(B^TL^\dagger\omega))_i} = 1, \quad i \in \{1, \ldots, |\mathcal{E}|\}.$$

Proof: Statement G1. For an acyclic graph, we have that $\mathrm{Ker}(B) = \emptyset$. According to *Theorem 1*, there exists an equilibrium $\theta^* \in \overline{\Delta}_G(\gamma)$ if and only if condition **[S17]** is satisfied. In this case, we obtain $B^T\theta^* = \mathbf{arcsin}(B^TL^\dagger\omega)$. This completes the proof of statement G1.

Statement G2. In the homogeneous case, we have that $L = K(nI_n - \mathbf{1}_{n\times n})$ and $L^\dagger = \frac{1}{Kn}(I_n - \frac{1}{n}\mathbf{1}_{n\times n})$(ref. 3, lemma 3.13). Thus, the inequality condition **[S17]** can be equivalently rewritten as $\sin(\gamma) \geq \|B^TL^\dagger \cdot \omega\|_\infty = \frac{1}{Kn}\|B^T\omega\|_\infty$. According to Dörfler and Bullo (ref. 9, theorem 4.1), the Kuramoto model **[S2]** with homogeneous coupling $a_{ij} = K$ features an exponentially stable equilibrium $\theta^* \in \overline{\Delta}_G(\gamma)$, $\gamma \in [0, \pi/2[$, for all $\omega \in \boldsymbol{\Omega}$ if and only if the condition $K > \|B^T\omega\|_\infty/n$ is satisfied. This concludes the proof of statement G2.

Statement G3. For notational convenience, let $c \triangleq \Omega_1 - \Omega_2$. Then, for any $\boldsymbol{\Omega}^* \in \boldsymbol{\Omega}$ and for $\omega = L\boldsymbol{\Omega}^*$, we have that $B^TL^\dagger\omega = B^TL^\dagger L\boldsymbol{\Omega}^* = B^T\boldsymbol{\Omega}^*$ is a vector with components $\{-c, 0, +c\}$. Now, consider the solution $\psi = B^TL^\dagger\omega = B^T\boldsymbol{\Omega}^*$ to the auxiliary fixed-point equation **[S11]**, and notice that $\mathbf{arcsin}(\psi) = \mathbf{arcsin}(B^T\boldsymbol{\Omega}^*)$ has components $\{-\arcsin(c), 0, +\arcsin(c)\}$. In particular, we have that $\mathbf{arcsin}(\psi) \in \mathrm{Im}(B^T)$, and the exact synchronization condition from *Theorem 1* is satisfied if and only if $\|\psi\|_\infty = c \leq \sin(\gamma)$, which corresponds to condition **[S17]**. The cut-set property follows because $B^T\theta^* = \mathbf{arcsin}(\psi)$ has components $\{-\arcsin(c), 0, +\arcsin(c)\} = \{-\gamma, 0, +\gamma\}$. This concludes the proof of statement G3.

Statement G4. Because $\arcsin(x)/x = 1 + x^2/6 + \mathcal{O}(x)^4$, we have that $(\mathbf{arcsin}(B^TL^\dagger\omega))_i/(B^TL^\dagger\omega)_i = 1 + \mathcal{O}((B^TL^\dagger\omega)_i^2)$ for each component $i \in \{1, \ldots, |\mathcal{E}|\}$. Thus, in the limit $B^TL^\dagger\omega \to \mathbf{0}_{|\mathcal{E}|}$, it follows that $\mathbf{arcsin}(B^TL^\dagger\omega) \in \mathrm{Im}(B^T)$, and the cycle constraint $\mathbf{arcsin}(\psi) = \mathbf{arcsin}(B^TL^\dagger\omega + \psi_{\mathrm{hom}}) \in \mathrm{Im}(B^T)$ is met with $\psi_{\mathrm{hom}} = \mathbf{0}_{|\mathcal{E}|}$. For $B^TL^\dagger\omega \to \mathbf{0}_{|\mathcal{E}|}$, the norm constraint $\|B^TL^\dagger\omega\|_\infty \leq \sin(\gamma)$ is satisfied as well with $\gamma \searrow 0$, and we obtain[¶] for each $i \in \{1, \ldots, |\mathcal{E}|\}$ that

$$\lim_{B^TL^\dagger\omega \to \mathbf{0}_{|\mathcal{E}|}} (B^T\theta^*)_i / (\mathbf{arcsin}(B^TL^\dagger\omega))_i = 1.$$

This concludes the proof of statement G4 and *Theorem 2.* ■

Theorem 1 shows that the solvability of the fixed-point equation **[S17]** is inherently related to the cycle constraints. The following lemma establishes feasibility of a single cycle.

Lemma 4 (Single Cycle Feasibility). *Consider the Kuramoto model* **[S2]** *with a cycle graph* $G(\mathcal{V}, \mathcal{E}, A)$ *and* $\omega \in \mathbf{1}_n^\perp$. *Without loss of generality, assume that the edges are labeled by* $\{i, i+1\}(\mathrm{mod}\ n)$ *for* $i \in \{1, \ldots, n\}$ *and* $\mathrm{Ker}(B) = \mathrm{span}(\mathbf{1}_n)$. *Define* $x \in \mathbf{1}_n^\perp$ *and* $y \in \mathbb{R}^n_{>0}$ *uniquely by* $x \triangleq B^TL^\dagger\omega$ and $y_i \triangleq a_{i,(i+1)(\mathrm{mod}n)} > 0$ *for* $i \in \{1, \ldots, n\}$. *Let* $\gamma \in [0, \pi/2[$.

The following statements are equivalent:

(*i*) *There exists a locally exponentially stable equilibrium* $\theta^* \in \overline{\Delta}_G(\gamma)$.

(*ii*) *The function* $f : [\lambda_{\min}, \lambda_{\max}] \to \mathbb{R}$ *with domain boundaries* $\lambda_{\min} = \max_{i\in\{1,\ldots,n\}} \frac{-\sin(\gamma) - x_i}{y_i}$ *and* $\lambda_{\max} = \min_{i\in\{1,\ldots,n\}} \frac{\sin(\gamma) - x_i}{y_i}$, *and defined by* $f(\lambda) = \sum_{i=1}^n \arcsin(x_i + \lambda y_i)$, *satisfies* $f(\lambda_{\min}) < 0 < f(\lambda_{\max})$.

If both equivalent statements (*i*) *and* (*ii*) *are true, then* $B^T\theta^* = \mathbf{arcsin}(x + \lambda^* y)$, *where* $\lambda^* \in [\lambda_{\min}, \lambda_{\max}]$ *satisfies* $f(\lambda^*) = 0$.

Proof: According to *Theorem 1*, there exists a locally exponentially stable equilibrium $\theta^* \in \overline{\Delta}_G(\gamma)$ if and only if there exists a solution $\psi = x + \lambda y$, $\lambda \in \mathbb{R}$, to the auxiliary fixed-point equation **[S11]** satisfying the norm constraint $\|\psi\|_\infty \leq \sin(\gamma)$ and the cycle constraint $\mathbf{arcsin}(\psi) \in \mathrm{Im}(B^T)$.

Equivalently, because $\mathrm{Ker}(B) = \mathrm{span}(\mathbf{1}_n)$, there is $\lambda \in \mathbb{R}$ satisfying the norm constraint $\|x + \lambda y\|_\infty \leq \sin(\gamma) < 1$ and the cycle constraint $\mathbf{1}_n^T \mathbf{arcsin}(x + y\lambda) = 0$. Equivalently, the function $f(\lambda) = \mathbf{1}_n^T \mathbf{arcsin}(x + y\lambda)$ features a zero $\lambda^* \in [\lambda_{\min}, \lambda_{\max}]$ (corresponding to the cycle constraint), where the constraints on $\lambda_{\min}$ and $\lambda_{\max}$ guarantee the norm constraints $x_i + y_i\lambda_{\max} \leq \sin(\gamma)$ and $x_i + y_i\lambda_{\min} \geq -\sin(\gamma)$ for all $i \in \{1, \ldots, n\}$. Equivalently, by the intermediate value theorem and due to continuity and (strict) monotonicity of the function f, we have that $f(\lambda_{\min}) < 0 < f(\lambda_{\max})$. Finally, if $\lambda^* \in [\lambda_{\min}, \lambda_{\max}]$ is found such that $f(\lambda^*) = 0$, by *Theorem 1*, $B^T\theta^* = \mathbf{arcsin}(\psi) = \mathbf{arcsin}(x + \lambda^* y)$. ■

Lemma 4 offers a checkable synchronization condition for cycles, which leads to the following theorem.

Theorem 3 (Synchronization Conditions for Cycle Graphs). *Consider the Kuramoto model* **[S2]** *with a cycle graph* $G(\mathcal{V}, \mathcal{E}, A)$ *and* $\omega \in \mathbf{1}_n^\perp$. *Consider the inequality condition* **[S17]** *for* $\gamma \in [0, \pi/2[$.

The following statements hold:

C1) **Exact synchronization condition for symmetrical natural frequencies:** *Assume that* $\omega \in \mathbf{1}_n^\perp$ *is such that* $B^TL^\dagger\omega$ *is a symmetrical vector.*[‖] *There is a locally exponentially stable equilibrium* $\theta^* \in \overline{\Delta}_G(\gamma)$ *if and only if condition* **[S17]** *holds. Moreover, in this case,* $B^T\theta^* = \mathbf{arcsin}(B^TL^\dagger\omega)$.

C2) **Tight synchronization condition for low-dimensional cycles:** *Assume the network contains* $n \in \{3, 4\}$ *oscillators. Consider a compact interval* $\Omega \subset \mathbb{R}$, *and let* $\boldsymbol{\Omega} = (\boldsymbol{\Omega}_1, \ldots, \boldsymbol{\Omega}_n) \subset \mathbb{R}^n$ *be the set of vectors with components* $\boldsymbol{\Omega}_i \in \Omega$ *for all* $i \in \{1, \ldots, n\}$. *For all* $\omega \in L\boldsymbol{\Omega}$, *there exists a locally exponentially stable equilibrium* $\theta^* \in \overline{\Delta}_G(\gamma)$ *if and only if condition* **[S17]** *holds.*

C3) **General cycles and network parameters:** *In general, for* $n \geq 5$ *oscillators, condition* **[S16]** *does not guarantee the existence of an equilibrium* $\theta^* \in \Delta_G(\pi/2)$. *As a sufficient condition, there exists a locally exponentially stable equilibrium* $\theta^* \in \overline{\Delta}_G(\gamma)$, $\gamma \in [0, \pi/2[$, *if*

$$\|B^TL^\dagger\omega\|_\infty \leq \frac{\min_{\{i,j\}\in\mathcal{E}} a_{ij}}{\max_{\{i,j\}\in\mathcal{E}} a_{ij} + \min_{\{i,j\}\in\mathcal{E}} a_{ij}} \cdot \sin(\gamma). \qquad \textbf{[S18]}$$

Proof. To prove the statements of *Theorem 3* and to show the existence of an equilibrium $\theta^* \in \overline{\Delta}_G(\gamma)$, we invoke the equivalent formulation via the function $f(\lambda)$ as constructed in *Lemma 4*. In particular, we seek to prove the following statement:

Let $\lambda_{\min} = \max_{i\in\{1,\ldots,n\}} \frac{-\sin(\gamma) - x_i}{y_i}$ *and* $\lambda_{\max} = \min_{i\in\{1,\ldots,n\}} \frac{\sin(\gamma) - x_i}{y_i}$. *The function* $f : [\lambda_{\min}, \lambda_{\max}] \to \mathbb{R}$ *defined by* $f(\lambda) = \sum_{i=1}^n$

[¶]The limit $\|B^TL^\dagger\omega\|_\infty \to 0$ implies that the resulting equilibrium $\theta^* \in \overline{\Delta}_G(0)$ corresponds to phase synchronization $\theta_i = \theta_j$ for all $i, j \in \{1, \ldots, n\}$. The converse statement $\theta^* \in \overline{\Delta}_G(0) \Rightarrow \omega = \mathbf{0}_n$ is also true, and its proof can be found in the paper by Dörfler and Bullo (ref. 9, theorem 5.5).

[‖]A vector $x \in 1_n^\perp$ is *symmetrical* if its histogram is symmetrical, that is, up to permutation of its elements, x is of the form $x = [-c, +c]^T$ for n even and some vector $c \in \mathbb{R}^{n/2}$ and $x = [-c, 0, +c]^T$ for n odd and some $c \in \mathbb{R}^{(n-1)/2}$.

$\arcsin(x_i+\lambda y_i)$ *satisfies* $f(\lambda_{\min})<0<f(\lambda_{\max})$ *(equivalently, there is* $\lambda^*\in[\lambda_{\min},\lambda_{\max}]$ *such that* $f(\lambda^*)=0$*) if and only if the condition* $\|x\|_\infty=\|B^TL^\dagger\omega\|_\infty\le\sin(\gamma)$ *is satisfied.*

Statement C1. For a symmetrical vector $x=B^TL^\dagger\omega$, all odd moments about the (zero) mean vanish, that is, $\sum_{i=1}^n x_i^{2p+1}=0$ for $p\in\mathbb{N}_0$. Because the Taylor series of the arcsin about zero features only odd powers, we have $f(0)=\sum_{i=1}^n\arcsin(x_i)=\sum_{i=1}^n\sum_{p=0}^\infty\frac{(2p)!}{2^{2p}(p!)^2(2p+1)}x_i^{2p+1}=0$. Statement C1 follows then immediately from *Lemma 4*.

Statement C2. By statement C1, statement C2 is true if $B^TL^\dagger\omega$ is symmetrical. Statement C2 can then be proved in a combinatorial fashion by considering all deviations from symmetry arising for three or four oscillators. To continue, recall that $\arcsin(x)$ is a superadditive function for $x\in[0,1]$ and a subadditive function for $x\in[-1,0]$, that is, $\arcsin(x)+\arcsin(y)<\arcsin(x+y)$ for $x,y>0$ and $x+y\le1$, $\arcsin(x)+\arcsin(y)>\arcsin(x+y)$ for $x,y<0$ and $x+y\ge-1$, and $\arcsin(x)+\arcsin(y)=\arcsin(x+y)$ for $x=y=0$. We now consider each case $n\in\{3,4\}$ separately.

Proof of sufficiency for n = 3: Assume that $\|x\|_\infty\le\sin(\gamma)$. Because the case $f(\lambda=0)=\mathbf{1}_n^T\mathbf{arcsin}(x)=0$ for a symmetrical vector $x\in\mathbb{R}^3$ is already proved, we consider now the asymmetrical case $f(\lambda=0)=\mathbf{1}_n^T\mathbf{arcsin}(x)>0$ [the proof of the case $\mathbf{1}_n^T\mathbf{arcsin}(x)<0$ is analogous]. Necessarily, it follows that at least two elements of x are negative. If one element of x is 0, say $x_1=0$, we fall back into the symmetrical case $x_2=-x_3$; on the other hand, if only one element is negative, say $x_1<0$ and $x_2,x_3>0$, we arrive at a contradiction $f(\lambda=0)=\sum_{i=1}^n\arcsin(x_i)=-\arcsin(x_2+x_3)+\arcsin(x_2)+\arcsin(x_3)<0$ due to superadditivity and because $x_1=-x_2-x_3$. Hence, without loss of generality, let $x=[a+b,\,-a,\,-b]^T$, where $a,b>0$. By assumption, $\|x\|_\infty\le\sin(\gamma)$. It follows that $a+b\le\sin(\gamma)$, $a<\sin(\gamma)$, $b<\sin(\gamma)$, and $\lambda_{\min}=\max_{i\in\{1,\dots,n\}}\frac{-\sin(\gamma)-x_i}{y_i}<0$.

Due to superadditivity, $f(\lambda=0)=\mathbf{1}_n^T\mathbf{arcsin}(x)=\arcsin(a+b)-(\arcsin(a)+\arcsin(b))>0$. Now, we evaluate $f(\lambda)$ at the lower end of its domain $[\lambda_{\min},\lambda_{\max}]$ and obtain

$$f(\lambda_{\min})=\arcsin(a+b+y_1\lambda_{\min})+\arcsin(-a+y_2\lambda_{\min})+\arcsin(-b+y_3\lambda_{\min}). \quad \textbf{[S19]}$$

By the definition of $\lambda_{\min}$, at least one summand on the right-hand side of **[S19]** equals $-\gamma$. Furthermore, notice that the second and third summands are negative and that the first summand satisfies $\arcsin(a+b+y_1\lambda_{\min})\ge-\gamma$. If $\arcsin(a+b+y_1\lambda_{\min})=-\gamma$, clearly, $f(\lambda_{\min})<0$. In the other case, $\arcsin(a+b+y_1\lambda_{\min})>-\gamma$, it follows that

$$f(\lambda_{\min})<\underbrace{\arcsin(a+b+y_1\lambda_{\min})-\gamma}_{<0}+\underbrace{\max\{\arcsin(-a+y_2\lambda_{\min}),\arcsin(-b+y_3\lambda_{\min})\}<0}_{<0}.$$

Because $f(\lambda_{\min})<0<f(0)\le f(\lambda_{\max})$, it follows from *Lemma 4* that there exists a stable equilibrium $\theta^*\in\overline{\Delta}_G(\gamma)$. The sufficiency is proved for $n=3$.

Proof of sufficiency for n = 4: Assume that $\|x\|_\infty\le\sin(\gamma)$. Without loss of generality, let $\operatorname{argmax}_{i\{1,\dots,4\}}\{|x_i|\}$ be a singleton (otherwise, x is necessarily symmetrical) and let $x\in\mathbf{1}_n^\perp$ be such that $f(\lambda=0)=\mathbf{1}_n^T\mathbf{arcsin}(x)>0$ (the proof of the case $\mathbf{1}_n^T\mathbf{arcsin}(x)<0$ is analogous). Necessarily, it follows that at least two elements of x are negative. If only one element of x is negative, say $x_1<0$, and $x_2,x_3,x_4\ge0$, we arrive at a contradiction because $f(\lambda=0)=\sum_{i=1}^n\arcsin(x_i)=-\arcsin(x_2+x_3+x_4)+\arcsin(x_2)+\arcsin(x_3)+\arcsin(x_4)$ is 0 only in the symmetrical case (e.g., $x_2=x_3=0<x_4=-x_1$) and is strictly negative otherwise (due to superadditivity). If exactly one element of x is positive (and three are nonpositive), say $x=[a+b+c,\,-a,\,-b,\,-c]^T$ for $a,b,c\ge0$ and $a+b+c=\|x\|_\infty\le\sin(\gamma)$, an analogous reasoning to the case $n=3$ leads to $f(\lambda_{\min})<0$.

It remains to consider the case of two positive and two negative entries. Without loss of generality, let $x_1\ge x_2>0>x_3\ge x_4$, where $x_1\ne-x_4$ and $x_2\ne-x_3$ (this is the symmetrical case), $\sum_{i=1}^n x_i=0$, and $\|x\|_\infty\le\sin(\gamma)$ by assumption. It follows that $\lambda_{\min}=\max_{i\in\{1,\dots,n\}}\frac{-\sin(\gamma)-x_i}{y_i}\le0$. Because $f(\lambda=0)=\mathbf{1}_n^T\arcsin(x)>0$ and $\mathbf{1}_n^Tx=0$, it follows from superadditivity that $\|x\|_\infty=\max\{x_1,x_2\}$, and the set $\operatorname{argmax}\{x_1,x_2\}$ must be a singleton (otherwise, we arrive again at a contradiction or at the symmetrical case). Suppose that $\|x\|_\infty=\max\{x_1,x_2\}=x_1$; then, necessarily $|x_2|<|x_3|\le|x_4|<|x_1|\le\sin(\gamma)$. It follows that $\lambda_{\min}<0$.

Again, we evaluate the sum $f(\lambda_{\min})=\sum_{i=1}^4\arcsin(x_i+y_i\lambda_{\min})$. Note that the last two summands, $\arcsin(x_3+y_3\lambda_{\min})$ and $\arcsin(x_4+y_4\lambda_{\min})$, are negative (because $0>x_3\ge x_4$ and $\lambda_{\min}<0$) and the first two summands satisfy $\min\{\arcsin(x_1+y_1\lambda_{\min}),\arcsin(x_2+y_2\lambda_{\min})\}\ge-\gamma$. If $\min\{\arcsin(x_1+y_1\lambda_{\min}),\arcsin(x_2+y_2\lambda_{\min})\}=-\gamma$, we have

$$f(\lambda_{\min})=\underbrace{\arcsin(x_3+y_3\lambda_{\min})+\arcsin(x_4+y_4\lambda_{\min})}_{<0}+\underbrace{(-\gamma+\max\{\arcsin(x_1+y_1\lambda_{\min}),\arcsin(x_2+y_2\lambda_{\min})\})}_{<0}<0.$$

In the case that $\min\{\arcsin(x_1+y_1\lambda_{\min}),\arcsin(x_2+y_2\lambda_{\min})\}>-\gamma$, we obtain $\min_{i\in\{3,4\}}\{\arcsin(x_i+y_i\lambda_{\min})\}=-\gamma$ and

$$f(\lambda_{\min})<\arcsin(x_1+y_1\lambda_{\min})+\arcsin(x_2+y_2\lambda_{\min})-\gamma+\max_{i\in\{3,4\}}\{\arcsin(x_i+y_i\lambda_{\min})\}.$$

Because $|x_2|<|x_3|\le|x_4|<|x_1|\le\sin(\gamma)$, it readily follows that $\arcsin(x_1+y_1\lambda_{\min})-\gamma<0$ and $\arcsin(x_2+y_2\lambda_{\min})+\max_{i\in\{3,4\}}\{\arcsin(x_i+y_i\lambda_{\min})\}<0$. We conclude that $f(\lambda_{\min})<0$. Because $f(\lambda_{\min})<0<f(0)\le f(\lambda_{\max})$, it follows from *Lemma 4* that there exists a stable equilibrium $\theta^*\in\overline{\Delta}_G(\gamma)$. The sufficiency is proved for $n=4$.

Proof of necessity for $n\in\{3,4\}$***:*** We prove the necessity by contradiction. Consider a compact cube $\mathcal{Q}=[-c,+c]^{|\mathcal{E}|}\subset\mathbb{R}^{|\mathcal{E}|}$, where $c>0$ satisfies $c>\sin(\gamma)$. Assume that for every $x\in\mathbf{1}_n^\perp$, even those satisfying $\|x\|_\infty\ge c$, there exists $\lambda\in\mathbb{R}$ such that the cycle constraint $\mathbf{1}_n^T\mathbf{arcsin}(x+\lambda y)=0$ and the norm constraint $\|x+\lambda y\|_\infty\le\sin(\gamma)$ are simultaneously satisfied. For the sake of contradiction, consider now the symmetrical case, where $x\in\mathbf{1}_n^\perp$ has components $x_i\in\{-c,+c,0\}$. As proved in statement C1, $\lambda^*=0$ uniquely solves the cycle constraint equation $0=f(\lambda^*=0)=\sum_{i=1}^n\arcsin(x_i+\lambda^*y)=\sum_{i=1}^n\arcsin(\pm c)$ for any value of $c\in[0,1]$. However, the norm constraint $\|x+\lambda^*y\|_\infty=\|x\|_\infty\le\sin(\gamma)$ can be satisfied only if $\|x\|_\infty\le\sin(\gamma)<c$. We arrive at a contradiction because we assumed $\|x\|_\infty\ge c>\sin(\gamma)$.

We conclude that if $x=B^TL^\dagger\omega$ is bounded within a compact cube $\mathcal{Q}=[-c,+c]^{|\mathcal{E}|}\subset\mathbb{R}^{|\mathcal{E}|}$ with $c\le\sin(\gamma)$, the condition **[S17]** is also necessary for synchronization of all considered parametric realizations of $B^TL^\dagger\omega$ within this compact cube $\mathcal{Q}$. For the compact set $\boldsymbol{\Omega}=\Omega^n\subset\mathbb{R}^n$, it follows that the image $B^TL^\dagger\cdot L\boldsymbol{\Omega}=B^T\boldsymbol{\Omega}$ equals the compact cube $\mathcal{Q}=[-(\max_{\omega\in\Omega}\omega-\min_{\omega\in\Omega}\omega),+(\max_{\omega\in\Omega}\omega-\min_{\omega\in\Omega}\omega)]^{|\mathcal{E}|}$. Hence, the condition **[S17]** is necessary for synchronization of all considered parametric realizations of ω in the compact set $L\boldsymbol{\Omega}$. This concludes the proof of statement C2.

Statement C3. To prove the first part of statement C3, we construct an explicit counterexample. Consider a cycle of length $n \geq 5$ with unit-weighed edges $a_{i,i+1} = 1$, and let

$$\omega = \alpha \cdot \left[1 + \frac{1}{n-3} \quad 0 \quad -2 \quad 1 - \frac{1}{n-3} \quad \mathbf{0}_{n-4} \right]^T,$$

where $\alpha \in [0, 1]$. For $\alpha < 1$, these parameters satisfy the necessary conditions [**S8** and **S9**]. For the given parameters, we obtain the nonsymmetrical vector $x = B^T L^\dagger \omega$ given by

$$x = B^T L^\dagger \omega = \alpha \cdot \left[-1 \quad -1 \quad 1 \quad \frac{1}{n-3} \mathbf{1}_{(n-3)} \right]^T. \qquad \textbf{[S20]}$$

Notice that $\|x\|_\infty = \alpha < 1$, x is nonsymmetrical and x is the minimum ∞-norm vector $\psi = x + \lambda \mathbf{1}_n$ for $\lambda \in \mathbb{R}$.

In the following, we will show that there exists no equilibrium in $\lim_{\gamma \uparrow \pi/2} \overline{\Delta}_G(\gamma) = \overline{\Delta}_G(\pi/2)$. Consider the function $f(\lambda) = \mathbf{arcsin}(\mathbf{1}_n^T x + \lambda \mathbf{1}_n)$ whose domain is centered symmetrically around 0, that is, $\lambda_{\max} = -\lambda_{\min} = \lim_{\gamma \uparrow \pi/2} (\sin(\gamma) - \alpha) = 1 - \alpha$. Note that the domain of f vanishes as $\alpha \uparrow 1$. For $n \to \infty$, we have that $\lim_{n\to\infty} f(0) = -\arcsin(\alpha) + \lim_{n\to\infty} (n-3) \cdot \arcsin(\alpha/(n-3)) = -\arcsin(\alpha) + \alpha$. Hence, because $n \to \infty$ and $\alpha \uparrow 1$, we obtain $f(0) = -\frac{\pi}{2} + 1 < 0$. Due to continuity of f with respect to α, n, and λ, we conclude that for $n \geq 5$ sufficiently large and $\alpha < 1$ sufficiently large, there is no λ^* such that $f(\lambda^*) = 0$. Hence, the condition $\|x\|_\infty = \|B^T L^\dagger \omega\|_\infty < 1$ does generally not guarantee the existence of $\theta^* \in \overline{\Delta}_G(\pi/2) \supset \Delta_G(\pi/2)$. A second numerical counterexample will be constructed in the example below.

A sufficient condition for the existence of an equilibrium $\theta^* \in \overline{\Delta}_G(\gamma)$ is $x_i + \lambda_{\min} y_i \leq 0 \leq x_i + \lambda_{\max} y_i$ for each $i \in \{1, \ldots, n\}$, which is equivalent to condition [**S18**] Indeed, if condition [**S18**] holds, we obtain $f(\lambda_{\min}) = \sum_{i=1}^n \arcsin(x_i + \lambda_{\min} y_i)$ as a sum of nonpositive terms and $f(\lambda_{\max}) = \sum_{i=1}^n \arcsin(x_i + \lambda_{\max} y_i)$ as a sum of nonnegative terms. Because $\mathbf{1}_n^T x = 0$ and generally $x \neq \mathbf{0}_n$ (otherwise we fall back into the symmetrical case), at least one x_i is strictly negative and at least one x_i is strictly positive, and it follows that $f(\lambda_{\min}) < 0 < f(\lambda_{\max})$. Statement C3 follows then immediately from *Lemma 4*. This concludes the proof. ■

In the following, define a *patched network* $\{G(\mathcal{V}, \mathcal{E}, A), \omega\}$ as a collection of subgraphs and natural frequencies $\omega \in \mathbf{1}_n^\perp$, where ($i$) each subgraph is connected; (ii) in each subgraph, one of the conditions G1, G2, G3, G4, C1, or C2 is satisfied; (iii) the subgraphs are connected to one another through edges $\{i,j\} \in \mathcal{E}$ satisfying $\|(e_i^{|\mathcal{E}|} - e_j^{|\mathcal{E}|})^T L^\dagger \omega\|_\infty \leq \sin(\gamma)$; and ($iv$) the set of cycles in the overall graph $G(\mathcal{V}, \mathcal{E}, A)$ is equal to the union of the cycles of all subgraphs. Because a patched network satisfies the synchronization condition [**S17**], as well the norm and cycle constraints, we can state the following result.

Corollary 1 (Synchronization Condition for a Patched Network). *Consider the Kuramoto model* [**S2**] *with a patched network* $\{G(\mathcal{V}, \mathcal{E}, A), \omega\}$, *and let* $\gamma \in [0, \pi/2[$. *There is a locally exponentially stable equilibrium* $\theta^* \in \overline{\Delta}_G(\gamma)$ *if condition* [**S17**] *holds.*

Example 1 (Numerical Cyclic Counterexample and Its Intuition). *In the proof of Theorem 3, we provided an analytical counterexample demonstrating that condition* [**S17**] *is not sufficiently tight for synchronization in sufficiently large cyclic networks. Here, we provide an additional numerical counterexample. Consider a cycle family of length* $n = 5 + 3 \cdot p$, *where* $p \in \mathbb{N}_0$ *is a nonnegative integer. Without loss of generality, assume that the edges are labeled by* $\{i, i+1\} (\text{mod } n)$ *for* $i \in \{1, \ldots, n\}$ *such that* $\text{Ker}(B) = \text{span}(\mathbf{1}_n)$. *Assume that all edges are unit-weighed* $a_{i,i+1 \ (\text{mod } n)} = 1$ *for* $i \in \{1, \ldots, n\}$. *Consider* $\alpha \in [0, 1[$, *and let*

$$\omega = \alpha \cdot \left[-1/2 \quad 2 \quad \mathbf{0}_{p+1} \quad 3/2 \quad \mathbf{0}_{2p+1} \right]^T.$$

For $n = 5$ $(p = 1)$, *the graph and the network parameters are illustrated in Fig. S5. For the given network parameters, we obtain the nonsymmetrical vector* $B^T L^\dagger \omega$ *given by*

$$B^T L^\dagger \omega = \alpha \cdot \left[1 \quad -1 \quad -\mathbf{1}_{(n-2)/3} \quad 1/2 \cdot \mathbf{1}_{2(n-2)/3} \right]^T.$$

Analogous to the example provided in the proof of Theorem 3, $\|B^T L^\dagger \omega\|_\infty = \alpha$ *and* $B^T L^\dagger \omega$ *is the minimum* ∞*-norm vector* $B^T L^\dagger \omega + \lambda \mathbf{1}_n$ *for* $\lambda \in \mathbb{R}$. *In the limit* $\alpha \uparrow 1$, *the necessary condition* [**S8**] *is satisfied with equality. In Fig. S5, for* $\alpha \uparrow 1$, *we have that* $\omega_2 = 2$, *and the necessary condition* [**S8**] *reads as* $a_{12} + a_{23} = |\omega_2| = 2$; *the corresponding equilibrium equation* $\sin(\theta_1 - \theta_2) + \sin(\theta_3 - \theta_2) = 2$ *can be satisfied only if* $\theta_1 - \theta_2 = \pi/2$ and $\theta_3 - \theta_2 = \pi/2$. *Thus, with two fixed-edge differences, there is no more "wiggle room" to compensate for the effects of* ω_i, $i \in \{1, 3, 4, 5\}$. *As a consequence, there is no equilibrium* $\theta^* \in \overline{\Delta}_G(\pi/2)$ *for* $\alpha = 1$ *or, equivalently,* $\|B^T L^\dagger \omega\|_\infty = 1$. *Due to continuity of the equations* [**S6**] *with respect to* α, *we conclude that for* $\alpha < 1$ *sufficiently large, there is no equilibrium either. Numerical investigations show that this conclusion is true, especially for very large cycles. For the extreme case* $p = 10^7$, *we obtain the critical threshold* $\alpha \approx 0.9475$, *where* $\theta^* \in \overline{\Delta}_G(\pi/2)$ *ceases to exist.*

Notice that both the counterexample used in the proof of *Theorem 3* and the one provided in *Example 1* are at the boundary of the admissible parameter space, where the necessary condition [**S8**] is marginally satisfied. In the next section, we establish that such "degenerate" counterexamples almost never occur for generic network topologies and parameters.

To conclude this section, we remark that the main technical difficulty in proving sufficiency of the condition [**S17**] for arbitrary graphs is the compact state space $\mathbb{T}^n$ and the nonmonotone sinusoidal coupling among the oscillators. Indeed, if the state space was $\mathbb{R}^n$ and if the oscillators were coupled via nondecreasing and odd functions, the synchronization problem would be simplified tremendously and the counterexamples in the proof of *Theorem 3* and in *Example 1* would not occur [an elegant analysis based on optimization theory is presented by Bürger et al. (46)].

Robust Synchronization in the Presence of Uncertainty

To evaluate the synchronization condition [**S17**], all network parameters a_{ij} and ω_i need to be known exactly. In many applications, this global knowledge is an unrealistic assumption and the network parameters may be uncertain, or even not constant over time. For instance, in power networks, the load and generation profiles $P_{\mathrm{m},i}$ and $P_{\mathrm{l},i}$, as well as the voltage magnitudes $|V_i|$, may be known only with a certain degree of accuracy; they have underlying unmodeled (or even unknown) dynamics; and they can be regarded as constant only over short time intervals. Hence, the associated natural frequencies ω_i and the coupling weights $a_{ij} = |V_i| \cdot |V_j| \cdot \Im(Y_{ij})$ are known only within certain ranges, and a synchronization test should be robust with respect to parametric variations.

In the following, we take parametric uncertainties into account and extend the synchronization condition [**S17**] to interval-valued network parameters. We consider a set of interval-valued natural frequencies defined by

$$\boldsymbol{\Omega} = \left\{ \omega \in \mathbf{1}_n^\perp : \underline{\omega_i} \leq \omega_i \leq \overline{\omega_i} \ \ \forall i \in \{1, \ldots, n\} \right\},$$

that is, for a vector $\omega \in \mathbf{\Omega}$, each entry is subject to upper and lower bounds. Accordingly, consider a set of edge weights defined by the interval-valued adjacency matrix**

$$\mathcal{A} = \Big\{ A \in \mathbb{R}^{n \times n} : 0 < \underline{a_{ij}} \le a_{ij} = a_{ji} \le \overline{a_{ij}} \ \forall \{i,j\} \in \mathcal{E}, \\ a_{ij} = a_{ji} = 0 \, \forall \, \{i,j\} \notin \mathcal{E} \Big\}.$$

Notice that both $\mathbf{\Omega}$ and $\mathcal{A}$ are convex sets and simply hypercubes in the vector spaces $\mathbf{1}_n^{\perp}$ and $\mathbb{R}^{n \times n}$. We define the associated discrete sets of vertices of $\mathbf{\Omega}$ and $\mathcal{A}$ by

$$\begin{aligned} \mathrm{vert}(\mathbf{\Omega}) &= \left\{ \omega \in \mathbf{1}_n^{\perp} : \omega_i \in \left\{ \underline{\omega_i}, \overline{\omega_i} \right\} \forall\, i \in \{1, \ldots, n\} \right\} \\ \mathrm{vert}(\mathcal{A}) &= \left\{ A \in \mathbb{R}^{n \times n} : a_{ij} = a_{ji} \in \left\{ \underline{a_{ij}}, \overline{a_{ij}} \right\} \forall \, \{i,j\} \in \mathcal{E} \right. \\ &\qquad \left. a_{ij} = a_{ji} = 0 \ \ \forall \{i,j\} \notin \mathcal{E} \right\}. \end{aligned}$$

Accordingly, consider the associated interval-valued Laplacian

$$\mathcal{L} = \left\{ L \in \mathbb{R}^{n \times n} : L = \mathrm{diag}\left(\left\{ \sum_{j=1}^{n} a_{ij} \right\}_{i=1}^{n} \right) - A, \, A \in \mathcal{A} \right\}$$

and its discrete vertex set

$$\mathrm{vert}(\mathcal{L}) = \left\{ L \in \mathbb{R}^{n \times n} : L = \mathrm{diag}\left(\left\{ \sum_{j=1}^{n} a_{ij} \right\}_{i=1}^{n} \right) - A, \, A \in \mathrm{vert}(\mathcal{A}) \right\}.$$

In the following, denote the convex hull of a set $\mathcal{S}$ by $\mathrm{conv}(\mathcal{S})$. By construction, we have that $\mathbf{\Omega} = \mathrm{conv}(\mathrm{vert}(\mathbf{\Omega}))$, $\mathcal{A} = \mathrm{conv}(\mathrm{vert}(\mathcal{A}))$, and $\mathcal{L} = \mathrm{conv}(\mathrm{vert}(\mathcal{L}))$.

Next, we consider a connected interval-valued network $\{G(\mathcal{V}, \mathcal{E}, \mathcal{A}), \omega\}$ with $A \in \mathcal{A}$ and $\omega \in \mathbf{\Omega}$. Consider the associated *interval-valued Laplacian equation*

$$Lx = \omega, \qquad \textbf{[S21]}$$

where $x \in \mathbf{1}_n^{\perp}$ is a variable and $L \in \mathcal{L}$ and $\omega \in \mathbf{\Omega}$ are parameters. The set of solutions $x \in \mathcal{X}$ to **[S21]** is given by

$$\mathcal{X} = \left\{ x \in \mathbf{1}_n^{\perp} : x = L^{\dagger} \omega, L \in \mathcal{L}, \omega \in \mathbf{\Omega} \right\}.$$

Accordingly, define the associated discrete vertex set

$$\mathrm{vert}(\mathcal{X}) = \left\{ x \in \mathbf{1}_n^{\perp} : x = L^{\dagger} \omega, L \in \mathrm{vert}(\mathcal{L}), \omega \in \mathrm{vert}(\mathbf{\Omega}) \right\}.$$

The following lemma for interval-valued linear systems is known for nonsingular and interval-valued M-matrices (47) and circuit-tableau matrices (48, 49). To best of our knowledge, this result is unknown for Laplacian matrices (corresponding to singular M-matrices or circuit-tableau matrices).

Lemma 5 (Interval-Valued Laplacian Equations). *Consider the interval-valued Laplacian equation* **[S21]**. *The set of solutions $\mathcal{X}$ is contained in the convex hull of its vertex set $\mathrm{vert}(\mathcal{X})$, that is, $\mathrm{conv}(\mathcal{X}) = \mathrm{conv}(\mathrm{vert}(\mathcal{X}))$.*

Proof: We first analyze the interval-valued Laplacian equation **[S21]** for the case that $\mathbf{\Omega}$ is a singleton, that is, we consider a fixed value of $\omega \in \mathbf{1}_n^{\perp}$ and parametric variations of $L \in \mathcal{L}$. According to Dörfler and Bullo (ref. 3, lemma III.9), we have for any Laplacian L corresponding to a connected, undirected, and weighted graph and for any arbitrary constant $\delta \neq 0$ that

$$(L + (\delta/n)\mathbf{1}_{n \times n})^{-1} = L^{\dagger} + (1/\delta n)\mathbf{1}_{n \times n}.$$

Consequently, for any $L \in \mathcal{L}$ and $\omega \in \mathbf{1}_n^{\perp}$, we have that

$$\begin{aligned} x &= L^{\dagger}\omega = \left(L^{\dagger} + (1/\delta n)\mathbf{1}_{n \times n}\right)\omega \\ &= (L + (\delta/n)\mathbf{1}_{n \times n})^{-1}\omega \\ &= \underbrace{\left(\sum_{\{i,j\} \in \mathcal{E}} a_{ij} \left(e_i^n - e_j^n\right) \cdot \left(e_i^n - e_j^n\right)^T + (\delta/n)\mathbf{1}_n \mathbf{1}_n^T \right)^{-1}}_{=Q} \omega. \end{aligned}$$

Thus, $x \in \mathbf{1}_n^{\perp}$ is the solution to the equation $Qx = \omega$, where Q is a regular interval-valued matrix, and in each parametric variation $0 < \underline{a_{ij}} \le a_{ij} = a_{ji} \le \overline{a_{ij}}$, $\{i,j\} \in \mathcal{E}$ enters additively via a rank-one matrix. Hence, the regularity assumptions of the interval-valued analyses in the study by Brayton et al. (ref. 48, theorem 1) and Dreyer (ref. 49, theorem 4.2) are satisfied, and we conclude that $\mathrm{conv}(\mathcal{X}) = \mathrm{conv}(\mathrm{vert}(\mathcal{X}))$.

Next, consider the case that $\mathcal{L}$ is a singleton, that is, we consider only variations of $\omega \in \mathbf{\Omega}$. Recall that $L^{\dagger}$ is a Laplacian matrix corresponding to a connected, undirected, and weighted graph (3) with weights $\tilde{a}_{ij} = \tilde{a}_{ji}$. In general, these edge weights $\tilde{a}_{ij}$ can be negative. In the interest of space, we restrict ourselves to nonnegative weights $\tilde{a}_{ij} = \tilde{a}_{ji} \ge 0$ here, but the following reasoning can be easily adapted to negative edge weights. Hence, for any $\omega \in \mathbf{\Omega}$, we obtain

$$x = L^{\dagger}\omega = \begin{bmatrix} \sum_{j=1}^{n} \tilde{a}_{1j}(\omega_1 - \omega_j) \\ \vdots \\ \sum_{j=1}^{n} \tilde{a}_{nj}(\omega_n - \omega_j) \end{bmatrix} \preceq \begin{bmatrix} \sum_{j=1}^{n} \tilde{a}_{1j}\left(\overline{\omega_1} - \underline{\omega_j}\right) \\ \vdots \\ \sum_{j=1}^{n} \tilde{a}_{nj}\left(\overline{\omega_n} - \underline{\omega_j}\right) \end{bmatrix},$$

$$x = L^{\dagger}\omega = \begin{bmatrix} \sum_{j=1}^{n} \tilde{a}_{1j}(\omega_1 - \omega_j) \\ \vdots \\ \sum_{j=1}^{n} \tilde{a}_{nj}(\omega_n - \omega_j) \end{bmatrix} \succeq \begin{bmatrix} \sum_{j=1}^{n} \tilde{a}_{1j}\left(\underline{\omega_1} - \overline{\omega_j}\right) \\ \vdots \\ \sum_{j=1}^{n} \tilde{a}_{nj}\left(\underline{\omega_n} - \overline{\omega_j}\right) \end{bmatrix},$$

where $\preceq$ and $\succeq$ denote the component-wise inequalities. This direct inspection shows that for fixed L, we have that $\mathrm{conv}(\mathcal{X}) = \mathrm{conv}(\mathrm{vert}(\mathcal{X}))$, that is, the extremal values of the solution x are achieved for extremal parameters $\omega \in \mathrm{vert}(\mathbf{\Omega})$.

Because the parametric variations $L \in \mathcal{L}$ and $\omega \in \mathbf{\Omega}$ are independent of each other, the lemma follows. ■

We obtain the following corollary to *Lemma 5*.

Corollary 2 (Extremal Solutions for Extremal Parameters). *Consider the interval-valued Laplacian equation* **[S21]** *and let $c \in \mathbb{R}^n$. Then, extremal values for $c^T x = c^T L^{\dagger}\omega$ are obtained for extremal parameters, that is,*

$$\max_{L \in \mathcal{L}, \omega \in \mathbf{\Omega}} c^T L^{\dagger}\omega = \max_{L \in \mathrm{vert}(\mathcal{L}), \omega \in \mathrm{vert}(\mathbf{\Omega})} c^T L^{\dagger}\omega,$$

$$\min_{L \in \mathcal{L}, \omega \in \mathbf{\Omega}} c^T L^{\dagger}\omega = \min_{L \in \mathrm{vert}(\mathcal{L}), \omega \in \mathrm{vert}(\mathbf{\Omega})} c^T L^{\dagger}\omega.$$

**The following analysis can be easily extended to the case of zero edge weights implying a nonconstant edge set $\mathcal{E}$ as long as the associated graph remains connected. Because the resulting notation is cumbersome and the combinatorial insights are not very surprising, we omit it here.

Proof: The proof is based on the analysis by Brayton et al. (ref. 48, theorem 2). We prove only the maximizing case here. The proof for the minimizing case can be obtained analogously.

Because the sets $\mathcal{L}$ and $\mathbf{\Omega}$ are compact and $c^T L^\dagger \omega$ is a continuous function[††] of $\omega \in \mathbf{\Omega}$ and $L \in \mathcal{L}$, the function $c^T L^\dagger \omega$ attains its maximum for some $\omega^* \in \mathbf{\Omega}$ and $L^* \in \mathcal{L}$.

By *Lemma 5*, there exist matrices $L_1, \ldots, L_{|\mathcal{E}|} \in \text{vert}(\mathcal{L})$, vectors $v_1, \ldots, v_n \in \text{vert}(\mathbf{\Omega})$, and nonnegative numbers $\lambda_1, \ldots, \lambda_{|\mathcal{E}|}$, $\mu_1, \ldots, \mu_n$ with $\sum_{i=1}^{|\mathcal{E}|} \lambda_i = 1$ and $\sum_{j=1}^{n} \mu_j = 1$ such that $(L^*)^\dagger = \sum_{i=1}^{|\mathcal{E}|} \lambda_i L_i^\dagger$ and $\omega^* = \sum_{j=1}^{n} \mu_j v_j$. It follows that

$$\begin{aligned} c^T (L^*)^\dagger \omega^* &= c^T \left(\sum_{i=1}^{|\mathcal{E}|} \lambda_i L_i^\dagger \right) \sum_{j=1}^{n} \mu_j v_j \\ &= \sum_{i=1}^{|\mathcal{E}|} \sum_{j=1}^{n} \lambda_i \mu_j \left(c^T L_i^\dagger v_j \right) \\ &\leq \max_{i \in \{1, \ldots, |\mathcal{E}|\}, j \in \{1, \ldots, n\}} c^T L_i^\dagger v_j, \end{aligned}$$

because any weighted average of numbers is bounded from above by the largest of the numbers. Thus, $\max_{L \in \mathcal{L}, \omega \in \mathbf{\Omega}} c^T L^\dagger \omega$ is attained at a vertex of the parameter space. ■

We are now ready to state the main result of this section. Specifically, if we can guarantee the synchronization condition **[S17]** for extremal parameters, we can guarantee synchronization for all parametric variations, and vice versa.

Theorem 4 (Robust Synchronization). *Consider a connected network* $\{G(\mathcal{V}, \mathcal{E}, \mathcal{A}), \omega\}$ *with interval-valued weights* $A \in \mathcal{A}$ *and natural frequencies* $\omega \in \mathbf{\Omega}$. *Let* $\mathcal{L}$ *be the associated set of interval-valued Laplacian matrices, and let* $\gamma \in [0, \pi/2[$.

The following statements are equivalent:

1) *Parametric synchronization condition:*

$$\left\| B^T L^\dagger \omega \right\|_\infty \leq \sin(\gamma) \quad \forall\ L \in \mathcal{L}, \quad \omega \in \mathbf{\Omega} \qquad \textbf{[S22]}$$

2) *Worst-case synchronization condition:*

$$\max_{L \in \text{vert}(\mathcal{L}), \omega \in \text{vert}(\mathbf{\Omega})} \left\| B^T L^\dagger \omega \right\|_\infty \leq \sin(\gamma) \qquad \textbf{[S23]}$$

Proof: The kth row of B^T reads as $b_k^T = e_i^n - e_j^n$, where $\{i,j\} \in \mathcal{E}$. Thus, condition **[S22]** is true if and only if

$$\begin{aligned} \sin(\gamma) \geq \max_{L \in \mathcal{L}, \omega \in \mathbf{\Omega}} \left\| B^T L^\dagger \omega \right\|_\infty &= \max_k \max_{L \in \mathcal{L}, \omega \in \mathbf{\Omega}} \left| b_k^T L^\dagger \omega \right| \\ &= \max_k \max_{L \in \text{vert}(\mathcal{L}), \omega \in \text{vert}(\mathbf{\Omega})} \left| b_k^T L^\dagger \omega \right| \\ &= \max_{L \in \text{vert}(\mathcal{L}), \omega \in \text{vert}(\mathbf{\Omega})} \left\| B^T L^\dagger \omega \right\|_\infty, \end{aligned}$$

where the second equality follows from *Corollary 2*. The latter statement is equivalent to condition **[S23]**. ■

The robust synchronization condition **[S23]** in *Theorem 4* is exact, but its evaluation is computationally expensive because all vertices of the parameter-space need to be sampled in a combinatorial way. We found that randomized Monte Carlo sampling methods or simplex-type algorithms perform well in practice and quickly deliver an accurate estimate of the quantity $\max_{L \in \text{vert}(\mathcal{L}), \omega \in \text{vert}(\mathbf{\Omega})} \| B^T L^\dagger \omega \|_\infty$. For certain topologies, such as acyclic ones, it is also possible to determine analytically the maximizing vertices beforehand, and the combinatorial condition **[S23]** reduces to a scalar one. In the subsection on *Synchronization Assessment for Power Networks*, *Theorem 4* is illustrated with different examples.

[††]Continuity of $L^\dagger \omega$ with respect to the weights a_{ij} follows because $L^\dagger \omega = Q^{-1} \omega$, Q is a continuous function of a_{ij}, and the inverse of a matrix is a continuous function of its elements.

Statistical Synchronization Assessment

After having established that the synchronization condition **[S17]** is necessary and sufficient for particular network topologies and parameters, we now validate both its correctness and its accuracy for arbitrary networks.

Statistical Assessment of Correctness. Extensive simulation studies lead us to the conclusion that condition **[S17]** is correct in general and guarantees the existence of a stable equilibrium $\theta^* \in \overline{\Delta}_G(\gamma)$. To validate this hypothesis, we invoke probability estimation through Monte Carlo techniques; see ref. 50, section 9 and ref. 51, section 3 for a comprehensive review.

We consider the following *nominal random networks* $\{G(\mathcal{V}, \mathcal{E}, \mathcal{A}), \omega\}$ parametrized by the number $n \geq 2$ of nodes, the width $\alpha > 0$ of the sampling region for each natural frequency ω_i, $i \in \{1, \ldots, n\}$, and a connected random graph model $\text{RGM}(p) = G(\mathcal{V}, \mathcal{E}(p))$ with node set $\mathcal{V} = \{1, \ldots, n\}$ and edge set $\mathcal{E} = \mathcal{E}(p)$ induced by a coupling parameter $p \in [0, 1]$. In particular, given the four parameters (n, RGM, p, α), a nominal random network is constructed as follows:

(*i*) *Network topology:* To construct the network topology, we consider three different one-parameter families of random graph models $\text{RGM}(p) = G(\mathcal{V}, \mathcal{E}(p))$, each parameterized by the number of nodes $n \geq 2$ and a coupling parameter $p \in [0, 1]$. Specifically, we consider (*a*) an Erdös–Rényi random graph model (RGM = ERG) with probability p of connecting two nodes, (*b*) a random geometric graph model (RGM = RGG) with sampling region $[0, 1]^2 \subset \mathbb{R}^2$ and connectivity radius p, and (*c*) a Watts–Strogatz small world network (RGM = SMN) (52) with initial coupling of each node to its two nearest neighbors and rewiring probability p. If, for a given $n \geq 2$ and $p \in [0, 1]$, the realization of an RGM is not connected, this realization is discarded and a new realization is constructed.

(*ii*) *Coupling weights:* For a given random graph $G(\mathcal{V}, \mathcal{E}(p))$, for each edge $\{i,j\} \in \mathcal{E}(p)$, the coupling weight $a_{ij} = a_{ji} > 0$ is sampled from a uniform distribution supported on the interval $[1, 10]$.

(*iii*) *Natural frequencies:* For a given $n \geq 2$ and $\alpha > 0$, the natural frequencies $\omega \in \mathbf{1}_n^\perp$ are constructed in two steps. In a first step, n real numbers q_i, $i \in \{1, \ldots, n\}$, are sampled from a uniform distribution supported on $[-\alpha, +\alpha]$, where $\alpha > 0$. In a second step, by subtracting the average $\sum_{i=1}^{n} q_i / n$, we define $\omega_i = q_i - \sum_{i=1}^{n} q_i / n$ for $i \in \{1, \ldots, n\}$ and obtain $\omega = (\omega_1, \ldots, \omega_n) \in \mathbf{1}_n^\perp$.

(*iv*) *Parametric realizations:* We consider 40 realizations of the parameter 4-tuple (n, RGM, p, α) covering a wide range of network sizes n, coupling parameters p, and natural frequencies ω, which are listed in the first column of Table S1. The choices of α in these 40 cases is such that[‡‡] the resulting equilibrium angles θ^* satisfy, on average, $\max_{\{i,j\} \in \mathcal{E}} |\theta_i^* - \theta_j^*| \approx \pi/3$.

[‡‡]For a fixed, weighted graph $G(\mathcal{V}, \mathcal{E}, A)$, the feasibility of **[S7]** and the properties of its solution θ^* are entirely determined by the remaining parameter $\alpha > 0$. If α is chosen too large, there exists no solution θ^* of the form $\max_{\{i,j\} \in \mathcal{E}} |\theta_i^* - \theta_j^*| \leq \pi/2$. Likewise, if α is chosen too small, $\omega \in 1_n^\perp$ will be nearly the zero vector and we fall into the case G4 of *Theorem 2*, that is, the angles are perfectly aligned. To strike a balance between these extreme cases, we choose α such that the samples yield, on average, $\max_{\{i,j\} \in \mathcal{E}} |\theta_i^* - \theta_j^*| \approx \pi/3$.

For each of the 40 parametric realizations in statement (*iv*), we generate 30,000 nominal models of $\omega \in \mathbf{1}_n^\perp$ and $G(\mathcal{V},\mathcal{E},A)$ (conditioned on connectivity) as detailed in statements (*i*)–(*iii*) above, each satisfying $\|B^T L^\dagger \omega\|_\infty < 1$. If a sample does not satisfy $\|B^T L^\dagger \omega\|_\infty < 1$, it is discarded and a new sample is generated. Hence, we obtain $1.2 \cdot 10^6$ *nominal random networks* $\{G(\mathcal{V},\mathcal{E},A),\omega\}$, each with a connected graph $G(\mathcal{V},\mathcal{E},A)$ and $\omega \in \mathbf{1}_n^\perp$ satisfying $B^T L^\dagger \omega_\infty \le \sin(\gamma)$ for some $\gamma < \pi/2$.

For each case and each instance, we numerically solve **[S7]** with an accuracy of 10^{-6} and test the hypothesis

$$\mathcal{H} : \left\|B^T L^\dagger \omega\right\|_\infty \le \sin(\gamma) \Rightarrow \exists\, \theta^* \in \overline{\Delta}_G(\gamma)$$

with an accuracy of 10^{-4}. The results are reported in Table S1, together with the empirical probability that the hypothesis $\mathcal{H}$ is true for a set of parameters (n, RGM, p, α). Given a set of parameters (n, RGM, p, α) and 30,000 samples, the empirical probability is calculated as

$$\widehat{\mathrm{Prob}}_{(n,\mathrm{RGM},p,\alpha)} = \frac{\text{number of samples satisfying}(\mathcal{H}\text{ is true})}{30,000}.$$

Given an accuracy level of $\epsilon \in]0,1[$ and a confidence level of $\eta \in]0,1[$, we ask for the number of samples N such that the true probability $\mathrm{Prob}_{(n,\mathrm{RGM},p,\alpha)}(\mathcal{H}$ is true) equals the empirical probability $\widehat{\mathrm{Prob}}_{(n,\mathrm{RGM},p,\alpha)}$ with a confidence level greater than $1-\eta$ and accuracy of at least ε, that is,

$$\mathrm{Prob}\left(\left|\mathrm{Prob}_{(n,\mathrm{RGM},p,\alpha)}(\mathcal{H}\text{ is true}) - \widehat{\mathrm{Prob}}_{(n,\mathrm{RGM},p,\alpha)}\right| < \epsilon\right) > 1-\eta.$$

By the Chernoff–Hoeffding bound (ref. 50, equation 9.14; ref. 53, theorem 1), the number of samples N for a given accuracy ϵ and confidence η is given as

$$N \ge \frac{1}{2\epsilon^2}\log\frac{2}{\eta}. \qquad \textbf{[S24]}$$

For $\epsilon = \eta = 0.01$, inequality **[S24]** is satisfied for $N \ge 26,492$ samples. By invoking the Chernoff–Hoeffding bound **[S24]**, our simulations studies establish the following statement:

With a 99% confidence level, there is at least 99% accuracy that the hypothesis $\mathcal{H}$ is true with a probability of 99.97% for a nominal network constructed as in statements (*i*)–(*iv*) *above*.

In particular, for a nominal network with parameters (n, RGM, p, α) constructed as in statements (*i*)–(*iv*) *above, with a 99% confidence level, there is at least 99% accuracy that the probability* $\mathrm{Prob}_{(n,\mathrm{RGM},p,\alpha)}$*($\mathcal{H}$ is true) equals the empirical probability* $\widehat{\mathrm{Prob}}_{(n,\mathrm{RGM},p,\alpha)}$, *as listed in Table S1, that is,*

$$\mathrm{Prob}\left(\left|\mathrm{Prob}_{(n,\mathrm{RGM},p,\alpha)}(\mathcal{H}\text{ is true}) - \widehat{\mathrm{Prob}}_{(n,\mathrm{RGM},p,\alpha)}\right| < 0.01\right) > 0.99.$$

It can be seen in Table S1 that the hypothesis $\mathcal{H}$ is always true for large and dense networks, whereas for small and sparsely connected networks, the hypothesis $\mathcal{H}$ can marginally fail with an error of order $\mathcal{O}(10^{-4})$. Thus, for these cases, a tighter condition of the form $\|B^T L^\dagger \omega\|_\infty \le \sin(\gamma) - \mathcal{O}(10^{-4})$ is required to establish the existence of $\theta^* \in \overline{\Delta}_G(\gamma)$. These results strongly suggest that degenerate topologies and parameters (e.g., the large and isolated cycles used in the proof of *Theorem 3* and in *Example 1*) are more likely to occur in small networks.

Statistical Assessment of Accuracy. As established in the previous section, the synchronization condition **[S17]** is a scalar synchronization test with predictive power for almost all network topologies and parameters. This remarkable fact is difficult to establish via statistical studies in the vast parameter space. Because we proved in statement G4 of *Theorem 2* that condition **[S17]** is exact for sufficiently small pairwise phase cohesiveness $|\theta_i - \theta_j| \ll 1$ (or, equivalently, for sufficiently identical natural frequencies ω_i and sufficiently strong coupling), we investigate the other extreme $\max_{\{i,j\}\in\mathcal{E}}|\theta_i - \theta_j| = \pi/2$. To test the corresponding synchronization condition **[S16]** in a low-dimensional parameter space, we consider a complex network of Kuramoto oscillators

$$\dot{\theta}_i = \omega_i - K \cdot \sum_{j=1}^{n} a_{ij}\sin(\theta_i - \theta_j), \quad i \in \{1,\ldots,n\}, \qquad \textbf{[S25]}$$

where $K > 0$ is the coupling gain among the oscillators and the coupling weights are assumed to be unit-weighted, that is, $a_{ij} = a_{ji} = 1$ for all $\{i,j\} \in \mathcal{E}$. If L is the unweighted Laplacian matrix, condition **[S16]** reads as $K > K_{\mathrm{critical}} \triangleq \|L^\dagger \omega\|_{\mathcal{E},\infty}$. Of course, the condition $K > K_{\mathrm{critical}}$ is only sufficient, and synchronization may occur for a smaller value of K than K_{critical}. To test the accuracy of the condition $K > K_{\mathrm{critical}}$, we numerically found the smallest value of K leading to synchrony for various network sizes, connected RGMs, and sample distributions of the natural frequencies. Here, we discuss in detail the construction of the random network topologies and parameters leading to the data displayed in Fig. 3.

We consider the following nominal random networks $\{G(\mathcal{V},\mathcal{E},A),\omega\}$ parametrized by the number of nodes $n \in \{10, 20, 40, 160\}$, the sampling distribution for the natural frequencies $\omega \in \mathbf{1}_n^\perp$, and a connected $\mathrm{RGM}(p) = G(\mathcal{V},\mathcal{E}(p))$ with node set $\mathcal{V} = \{1,\ldots,n\}$ and edge set $\mathcal{E} = \mathcal{E}(p)$ induced by a coupling parameter, $p \in [0,1]$. In particular, given the four parameters (n, RGM, p, α), a nominal random network is constructed as follows:

(*i*) *Network topology and weights:* To construct the network topology, we consider three different one-parameter families of $\mathrm{RGM}(p) = G(\mathcal{V},\mathcal{E}(p))$, each parameterized by the number of nodes n and a coupling parameter $p \in [0,1]$. Specifically, we consider (*a*) an ERG (RGM = ERG) with probability p of connecting two nodes, (*b*) a RGG (RGM = RGG) with sampling region $[0,1]^2 \subset \mathbb{R}^2$ and connectivity radius p, and (*c*) a Watts–Strogatz SMN (RGM = SMN) (52) with initial coupling of each node to its two nearest neighbors and rewiring probability p. If, for a given n and $p \in [0,1]$, the realization of an RGM is not connected, this realization is discarded and new realization is constructed. All nonzero coupling weights are set to 1, that is, $a_{ij} = a_{ji} = 1$ for $\{i,j\} \in \mathcal{E}$.

(*ii*) *Natural frequencies:* For a given network size n and sampling distribution, the natural frequencies $\omega \in \mathbf{1}_n^\perp$ are constructed in three steps. In a first step, the sampling distribution of the natural frequencies is chosen. For classic Kuramoto oscillators with uniform coupling $a_{ij} = K/n$ for distinct $i,j \in \{1,\ldots,n\}$, we know that the two extreme sampling distributions (with bounded support) are the bipolar (discrete) and uniform (flat) distribution leading to the largest critical coupling and smallest critical coupling, respectively (9). Here, we choose a uniform sampling distribution (SD = uniform) supported on $[-1,+1]$ or a bipolar discrete sampling distribution (SD = bipolar) supported on $\{-1,+1\}$. In a second step, n real numbers q_i, $i \in \{1,\ldots,n\}$, are sampled from the sampling distribution. In a third step, by subtracting the average $\sum_{i=1}^{n} q_i/n$, we define $\omega_i = q_i - \sum_{i=1}^{n} q_i/n$ for $i \in \{1,\ldots,n\}$ and obtain $\omega = (\omega_1,\ldots,\omega_n) \in \mathbf{1}_n^\perp$.

(*iii*) *Parametric realizations:* We consider 600 realizations of parameter 4-tuple (n, RGM, p, α) covering a wide range of network sizes n, coupling parameters p, and natural frequencies ω. All 600 realizations are shown in Fig. 3.

For each of the 600 parametric realizations in statement (*iii*), we generate 100 nominal models of $\omega \in \mathbf{1}_n^\perp$ and $G(\mathcal{V},\mathcal{E},A)$ (conditioned on connectivity) as detailed in statements (*i*) and (*ii*) above. Hence, we obtain 60,000 nominal random networks $\{G(\mathcal{V},\mathcal{E},A),\omega\}$, each with a connected graph $G(\mathcal{V},\mathcal{E},A)$ and natural frequencies $\omega \in \mathbf{1}_n^\perp$. For each sample network, we consider the complex Kuramoto model [**S25**] and numerically find the smallest value of K leading to synchrony with cohesive phases satisfying $\max_{\{i,j\}\in\mathcal{E}}|\theta_i-\theta_j| = \pi/2$. The critical value of K is found iteratively by integrating the Kuramoto dynamics [**S25**] and decreasing K if the steady-state θ^* satisfies $\max_{\{i,j\}\in\mathcal{E}}|\theta_i^*-\theta_j^*| < \pi/2$ and increasing K otherwise. We repeat this iteration until a steady-state θ^* is found satisfying $\max_{\{i,j\}\in\mathcal{E}}|\theta_i-\theta_j| = \pi/2$ with an accuracy of 10^{-3}. Our findings are reported in Fig. 3, where each data point corresponds to the sample mean of 100 nominal models with the same parameter 4-tuple (n, RGM, p, α).

Synchronization Assessment for Power Networks. We envision that our proposed condition [**S17**] can be applied to assess synchronization and robustness quickly in power networks under volatile operating conditions. Because real-world power networks are carefully engineered systems with particular network topologies and parameters, they cannot be reduced to the standard topological RGMs (54), and we do not extrapolate the statistical results from the previous section to power grids. Rather, we consider 10 widely established and commonly studied IEEE power network test cases provided by Zimmerman et al. (55) and Grigg et al. (56) to validate the correctness and the predictive power of our synchronization condition [**S17**].

Statistical Synchronization Assessment for IEEE Systems. We validate the synchronization condition [**S17**] in a smart power grid scenario subject to fluctuations in load and generation and equipped with fast-ramping generation and controllable demand. Here, we report the detailed simulation setup leading to the results shown in Table 1.

The nominal simulation parameters for the 10 IEEE test cases can be found in the studies by Zimmerman et al. (55) and Grigg et al. (56). Under nominal operating conditions, the power generation is optimized to meet the forecast demand while obeying the AC power flow laws and respecting the thermal limits of each transmission line. Thermal limit constraints are precisely equivalent to phase cohesiveness requirements, that is, for each line $\{i,j\}$, the angular distance $|\theta_i-\theta_j|$ needs to be bounded such that the corresponding power flow $a_{ij}\sin(\theta_i-\theta_j)$ is bounded. Here, we found the optimal generator power injections through the standard optimal power flow solver provided by MATPOWER (55).

To test the synchronization condition [**S17**] in a volatile smart grid scenario, we make the following changes to the nominal IEEE test cases with optimal generation:

(*i*) *Fluctuating loads with stochastic power demand:* We assume fluctuating demand and randomize 50% of all loads (selected independently with identical distribution) to deviate from the forecasted loads with Gaussian statistics (with nominal power injection as mean and standard deviation (SD) 0.3 per unit system).

(*ii*) *Renewables with stochastic power generation:* We assume that the grid is penetrated by renewables with severely fluctuating power outputs, for example, wind or solar farms, and we randomize 33% of all generating units (selected independently with identical distribution) to deviate from the nominally scheduled generation with Gaussian statistics (with nominal power injection as mean and SD 0.3 per unit system).

(*iii*) *Fast-ramping generation and controllable loads:* Following the paradigm of smart operation of smart grids (57), the fluctuations can be mitigated by fast-ramping generation, such as fast-response energy storage, including batteries and flywheels, and controllable loads, such as large-scale server farms or fleets of plug-in hybrid electrical vehicles. Here, we assume that the grid is equipped with 10% fast-ramping generation (10% of all generators, selected independently with identical distribution) and 10% controllable loads (10% of all loads, selected independently with identical distribution) and that the power imbalance (caused by fluctuating demand and generation) is uniformly dispatched among these adjustable power sources.

For each of the 10 IEEE test cases with optimal generator power injections, we construct 1,000 random realizations of the scenarios (*i*)–(*iii*) described above. For each realization, we numerically check for the existence of a solution $\theta^* \in \overline{\Delta}_G(\gamma)$, $\gamma \in [0,\pi/2[$, to the AC power flow equations, the right-hand side of the power network dynamics [**S4** and **S5**], given by

$$\begin{aligned} P_{\mathrm{m},i} &= \sum_{j=1}^{n} a_{ij}\sin(\theta_i-\theta_j), \quad i\in\mathcal{V}_1 \\ P_{\mathrm{l},i} &= -\sum_{j=1}^{n} a_{ij}\sin(\theta_i-\theta_j), \quad i\in\mathcal{V}_2. \end{aligned} \qquad [\mathbf{S26}]$$

The solution to the AC power flow equations [**S26**] is found via the AC power flow solver provided by MATPOWER (55). Notice that, by *Lemma 2*, if such a solution θ^* exists, it is unique (up to rotational invariance) and also locally exponentially stable with respect to the power network dynamics [**S4** and **S5**]. Next, we compare the numerical solution θ^* with the results predicted by our synchronization condition [**S17**]. As discussed in *Remark 3*, a physical insightful and computationally efficient way to evaluate condition [**S17**] is to solve the sparse and linear DC power flow equations given by

$$\begin{aligned} P_{\mathrm{m},i} &= \sum_{j=1}^{n} a_{ij}(\delta_i-\delta_j), \quad i\in\mathcal{V}_1 \\ P_{\mathrm{l},i} &= -\sum_{j=1}^{n} a_{ij}(\delta_i-\delta_j), \quad i\in\mathcal{V}_2. \end{aligned} \qquad [\mathbf{S27}]$$

The solution δ^* of the DC power flow equations [**S27**] is defined uniquely up to the usual translational invariance. Given the solution δ^* of the DC power flow equations [**S27**], the left-hand side of our synchronization condition [**S17**] evaluates to $\|B^T L^\dagger \omega\|_\infty = \|L^\dagger\omega\|_{\mathcal{E},\infty} = \max_{\{i,j\}\in\mathcal{E}}|\delta_i^*-\delta_j^*|$.

Finally, we compare our prediction with the numerical results. If $\|B^T L^\dagger\omega\|_\infty \le \sin(\gamma)$ for some $\gamma\in[0,\pi/2[$, condition [**S17**] predicts that there exists a stable solution $\theta\in\overline{\Delta}_G(\gamma)$ or, alternatively, $\theta\in\overline{\Delta}_G(\arcsin(\|B^TL^\dagger\omega\|_\infty))$. To validate this hypothesis, we compare the numerical solution θ^* with the AC power flow equations [**S26**] with our prediction $\theta^*\in\overline{\Delta}_G(\arcsin(\|B^TL^\dagger\omega\|_\infty))$. Our findings and the detailed statistics are reported in Table 1. It can be observed that condition [**S17**] predicts the correct phase cohesiveness $|\theta_i^*-\theta_j^*|$ along all transmission lines $\{i,j\}\in\mathcal{E}$ with extremely high accuracy even for large-scale networks, such as the Polish power grid model featuring 2,383 nodes.

Simulation Data for the RTS 96. The RTS 96 is a widely adopted and relatively large-scale power network test case, which has been designed as a benchmark model for power flow and stability studies. The RTS 96 is a multiarea model featuring 40 load buses and 33 generation buses, as illustrated in Fig. 4. The network parameters and the dynamic generator parameters can be found in the study by Grigg et al. (56).

The quantities a_{ij} in the coupled oscillator model [**S1**] correspond to the product of the voltage magnitudes at buses i and j, as well to the susceptance of the transmission line connecting buses i and j. For a given set of power injections at the buses and branch parameters, the voltage magnitudes and initial phase angles were calculated using the optimal power flow solver provided by MATPOWER (55). The quantities $\omega_i, i \in \mathcal{V}_2$, are the real-power demands at loads, and $\omega_i, i \in \mathcal{V}_1$, are the real-power injections at the generators, which were found through the optimal power flow solver provided by MATPOWER (55). We made the following changes to adapt the detailed RTS 96 model to the classic structure-preserving power network model [**S4** and **S5**] describing the generator rotor and voltage phase dynamics. First, we replaced the synchronous condenser in the original RTS 96 model (56) by a U50 hydrogenerator. Second, because the numerical values of the damping coefficients D_i are not contained in the original RTS 96 description (56), we chose the following values to be found in ref. 16: For the generator damping, we chose the uniform damping coefficient $D_i = 1$ per unit system and for $i \in \mathcal{V}_1$, and for the load frequency coefficient, we chose $D_i = 0.1$ s for $i \in \mathcal{V}_2$. Third and finally, we discarded an optional high-voltage DC link for the branch $\{113, 316\}$.

Bifurcation Scenario in the RTS 96. As shown in the main text, an imbalanced power dispatch in the RTS 96 network, together with a tripped generator (generator 323) in the southeastern (green) area, results in a loss of synchrony because the maximal power transfer is limited due to thermal constraints. This loss of synchrony can be predicted by our synchronization condition [**S17**] with extremely high accuracy. In the following, we show that a similar loss of synchrony occurs, even if the generator 323 is not disconnected and there are no thermal limit constraints on the transmission lines. In this case, the loss of synchrony is due to a saddle-node bifurcation at an interarea angle of $\pi/2$, which can be predicted accurately by condition [**S17**] as well.

For the following dynamic simulation, we consider again an imbalanced power dispatch. The demand at each load in the southeastern (green) area is increased by a uniform amount, and the resulting power imbalance is compensated for by uniformly increasing the generation at each generator in the northwestern (blue) area. The imbalanced power dispatch essentially transforms the RTS 96 into a two-oscillator network, and we observe the classic loss of synchrony through a saddle-node bifurcation (9, 18) shown in Figs. S6 and S7. In particular, the network is still synchronized for a load increase of 141%, resulting in $\|L^\dagger \omega\|_{\mathcal{E},\infty} = 0.9995 < 1$. If the loads are increased by an additional 10%, resulting in $\|L^\dagger \omega\|_{\mathcal{E},\infty} = 1.0560 > 1$, synchronization is lost and the areas separate via the transmission lines $\{121, 325\}$ and $\{223, 318\}$. In summary, this transmission line scenario nicely illustrates the correctness and the accuracy of the proposed condition [**S16**].

We want to make two remarks on this bifurcation scenario and its extensions to more detailed power network models. As discussed in *Remark 1*, the underlying modeling assumption of constant voltage magnitudes at the loads may not be true near the bifurcation point, and a higher order model, including voltage dynamics and reactive power flow equations, may reveal different dynamics than the considered model [**S4** and **S5**]. Additionally, in real-world power networks, the transmission lines $\{121, 325\}$ and $\{223, 318\}$ would be separated at some smaller interarea angle $\gamma^* \ll \pi/2$ due to thermal limit constraints on the transmission lines. This separation at the angle γ^* can also be predicted accurately from condition [**S17**], as discussed in the analysis and results in the main text.

Synchronization Assessment in the Presence of Nonconstant Voltages and Power Demands. As discussed in *Remark 1*, the underlying modeling assumption of constant voltage magnitudes at the loads is idealistic and not always true. For example, if the loads demand a constant amount of active and reactive power (rather than demanding constant power and voltage), the load bus voltages have to follow the power demand and the coupling weights $a_{ij} = |V_i| \cdot |V_j| \cdot \Im(Y_{ij})$ cannot be regarded as a priori known and constant parameters. Likewise, the active power demand ω_i at the loads is variable and can only be predicted with a certain accuracy.

In the following, we overapproximate uncertain parameters and unmodeled dynamics by the interval-valued parameters $\underline{\omega_i} \le \omega_i \le \overline{\omega_i}$ and $0 < \underline{a_{ij}} \le a_{ij} \le \overline{a_{ij}}$, and we apply the analysis developed in *SI Robust Synchronization in Presence of Uncertainty*. To verify the accuracy of the proposed robust synchronization condition [**S23**], we repeat similar numerical experiments as in the subsection on *Statistical Synchronization Assessment for IEEE Systems*. We consider four representative IEEE test cases of different sizes (nine-bus system by Chow, IEEE 14, IEEE 39 New England, and IEEE 118) with optimal generator power injections, and we make the following changes to these nominal test cases:

(*i*) *Fluctuating loads with stochastic active and reactive power demand:* We assume fluctuating demand and randomize all loads to deviate from their nominal values with Gaussian statistics, with nominal active and reactive power demands as mean, SD 0.3 (per unit system) for the reactive power demand, and SD 0.05 (per unit system) for the active power demand.

(*ii*) *Fast-ramping generation:* We assume that the grid is equipped with 20% fast-ramping generation (20% of all generators, selected independently with identical distribution) and the active power imbalance (caused by fluctuating demand) is uniformly dispatched among these adjustable power sources. Notice that the fast-ramping generators do not provide any reactive power support for the fluctuating reactive power demands at the loads, which results in highly variable load bus voltages.

For each of the four IEEE test cases, we construct 1,000 random realizations of scenarios (*i*) and (*ii*) described above. For each realization, we numerically check for the existence of a solution $\theta^* \in \overline{\Delta}_G(\gamma)$, $\gamma \in [0, \pi/2[$ to the active power flow equations [**S26**]. Here, the parameters $a_{ij} = |V_i| \cdot |V_j| \cdot \Im(Y_{ij})$ are found by solving the reactive power balance equations using MATPOWER (55). After obtaining all network samples and their solutions, we construct the left-hand side of our robust synchronization condition [**S23**], $\max_{L \in \mathrm{vert}(\mathcal{L}), \omega \in \mathrm{vert}(\boldsymbol{\Omega})} \|B^T L^\dagger \omega\|_\infty$. Next, we compare the numerical solution θ^* (obtained for each sample) with the robust synchronization condition [**S23**], which predicts that $\theta^* \in \overline{\Delta}_G(\arcsin(\max_{L \in \mathrm{vert}(\mathcal{L}), \omega \in \mathrm{vert}(\boldsymbol{\Omega})} \|B^T L^\dagger \omega\|_\infty))$. Our findings are reported are reported in Table S2.

First, observe from Table S2 that the load voltages and power injections fluctuate severely, and the resulting interval-valued parameters $\underline{\omega_i} \le \omega_i \le \overline{\omega_i}$ and $0 < \underline{a_{ij}} \le a_{ij} \le \overline{a_{ij}}$ are allowed to vary in relatively large domains. Despite these severe uncertainties, it can be observed that the robust synchronization condition [**S23**] still predicts the correct phase cohesiveness $|\theta_i^* - \theta_j^*|$ along all transmission lines $\{i, j\} \in \mathcal{E}$ with relatively high accuracy. Of course, the results in Table S2 are more conservative than those in Table 1 because condition [**S23**] is based on an overapproximation of the detailed power network dynamics, that is, certain vertices of the set $\{\mathrm{vert}(\mathcal{L}), \mathrm{vert}(\boldsymbol{\Omega})\}$ do not occur when numerically solving a detailed power network model, and they are the dominant source for the accuracy errors in Table S2.

These results show that the robust synchronization condition [**S23**] is indeed capable of predicting the solutions to the active power flow equations [**S26**] in presence of uncertain voltages (resulting from the unmodeled reactive power flow equations) and fluctuating loads. Conversely, if the voltage magnitudes

$|V_i|$ are known to vary within reasonable prespecified bounds (e.g., $|V_i| \in [0.95, 1.05]$) and the loads are predicted with high accuracy, condition **[S23]** delivers accurate results in the presence of uncertainties.

1. Biggs N *Algebraic Graph Theory* (1994) (Cambridge Univ Press, Cambridge, UK), Ed 2.
2. Biggs N (1997) Algebraic potential theory on graphs. *Bull Lond Math Soc* 29:641–683.
3. Dörfler F, Bullo F (2011) Kron reduction of graphs with applications to electrical networks. *IEEE Trans Circ Syst* 60(1):150–163.
4. Kuramoto Y (1975) Self-entrainment of a population of coupled non-linear oscillators. *International Symposium on Mathematical Problems in Theoretical Physics, Lecture Notes in Physics*, ed Araki H (Springer), Vol. 39, pp 420–422.
5. Kuramoto Y (1984) *Chemical Oscillations, Waves, and Turbulence* (Springer, New York, NY).
6. Strogatz SH (2000) From Kuramoto to Crawford: Exploring the onset of synchronization in populations of coupled oscillators. *Physica D* 143:1–20.
7. Acebrón JA, Bonilla LL, Vicente CJP, Ritort F, Spigler R (2005) The Kuramoto model: A simple paradigm for synchronization phenomena. *Rev Mod Phys* 77:137–185.
8. Winfree AT (2001) *The Geometry of Biological Time* (Springer, New York, NY), Ed 2.
9. Dörfler F, Bullo F (2011) On the critical coupling for Kuramoto oscillators. *SIAM J Appl Dyn Syst* 10:1070–1099.
10. Dörfler F, Bullo F (2012) Exploring synchronization in complex oscillator networks. *IEEE Conference on Decision and Control*. Available at http://arxiv.org/pdf/1209.1335.pdf. Accessed September 6, 2012.
11. Sauer PW, Pai MA (1998) *Power System Dynamics and Stability* (Prentice Hall, Englewood Cliffs, NJ).
12. Bergen AR, Hill DJ (1981) A structure preserving model for power system stability analysis. *IEEE Trans Power Apparatus Syst* 100:25–35.
13. Sastry S, Varaiya P (1980) Hierarchical stability and alert state steering control of interconnected power systems. *IEEE Trans Circ Syst* 27:1102–1112.
14. Chiang H-D, Chu CC, Cauley G (1995) Direct stability analysis of electric power systems using energy functions: Theory, applications, and perspective. *Proc IEEE* 83:1497–1529.
15. Dörfler F, Bullo F (2012) Synchronization and transient stability in power networks and non-uniform Kuramoto oscillators. *SIAM J Contr Optim* 50:1616–1642.
16. Kundur P (1994) *Power System Stability and Control* (McGraw-Hill, New York).
17. Simpson-Porco JW, Dörfler F, Bullo F (2012) Droop-controlled inverters in microgrids are Kuramoto oscillators. *IFAC Workshop on Distributed Estimation and Control in Networked Systems*, Santa Barbara, CA, pp 264–269, 10.3182/20120914-2-US-4030.00055.
18. Dobson I (1992) Observations on the geometry of saddle node bifurcation and voltage collapse in electrical power systems. *IEEE Trans Circ Syst I Fundam Theory Appl* 39:240–243.
19. Wu FF, Kumagai S (1980) *Limits on Power Injections for Power Flow Equations to Have Secure Solutions* (Electronics Research Laboratory, College of Engineering, University of California, Berkeley, CA).
20. Jadbabaie A, Motee N, Barahona M (2004) On the stability of the Kuramoto model of coupled nonlinear oscillators. *American Control Conference*, Boston, MA, pp 4296–4301. Available at http://ieeexplore.ieee.org/stamp/stamp.jsp?tp=&arnumber=1383983&isnumber=30144. Accessed June 30, 2004.
21. Nishikawa T, Motter AE, Lai YC, Hoppensteadt FC (2003) Heterogeneity in oscillator networks: Are smaller worlds easier to synchronize? *Phys Rev Lett* 91(1):014101.
22. Arenas A, Díaz-Guilera A, Kurths J, Moreno Y, Zhou C (2008) Synchronization in complex networks. *Phys Rep* 469:93–153.
23. Boccaletti S, Latora V, Moreno Y, Chavez M, Hwang DU (2006) Complex networks: Structure and dynamics. *Phys Rep* 424:175–308.
24. Wu F, Kumagai S (1982) Steady-state security regions of power systems. *IEEE Trans Circ Syst* 29:703–711.
25. Korniss G, et al. (2006) Scaling in small-world resistor networks. *Phys Lett A* 350:324–330.
26. Buzna L, Lozano S, Díaz-Guilera A (2009) Synchronization in symmetric bipolar population networks. *Phys Rev E Stat Nonlin Soft Matter Phys* 80(6 Pt 2):066120.
27. Pecora LM, Carroll TL (1998) Master stability functions for synchronized coupled systems. *Phys Rev Lett* 80:2109–2112.
28. Verwoerd M, Mason O (2008) Global phase-locking in finite populations of phase-coupled oscillators. *SIAM J Appl Dyn Syst* 7:134–160.
29. Strogatz SH, Mirollo RE (1988) Phase-locking and critical phenomena in lattices of coupled nonlinear oscillators with random intrinsic frequencies. *Physica D* 31:143–168.
30. Kopell N, Ermentrout GB (1988) Coupled oscillators and the design of central pattern generators. *Math Biosci* 90:87–109.
31. Verwoerd M, Mason O (2009) On computing the critical coupling coefficient for the Kuramoto model on a complete bipartite graph. *SIAM J Appl Dyn Syst* 8:417–453.
32. Gómez-Gardeñes J, Moreno Y, Arenas A (2007) Paths to synchronization on complex networks. *Phys Rev Lett* 98(3):034101.
33. Moreno Y, Pacheco AF (2004) Synchronization of Kuramoto oscillators in scale-free networks. *Europhys Lett* 68:603.
34. Kalloniatis AC (2010) From incoherence to synchronicity in the network Kuramoto model. *Phys Rev E Stat Nonlin Soft Matter Phys* 82(6 Pt 2):066202.
35. Strogatz SH (2001) Exploring complex networks. *Nature* 410(6825):268–276.
36. Tavora CJ, Smith OJM (1972) Stability analysis of power systems. *IEEE Trans Power Apparatus Syst* 91:1138–1144.
37. Tavora CJ, Smith OJM (1972) Equilibrium analysis of power systems. *IEEE Trans Power Apparatus Syst* 91:1131–1137.
38. Ilić M (1992) Network theoretic conditions for existence and uniqueness of steady state solutions to electric power circuits. *IEEE International Symposium on Circuits and Systems,* (San Diego, CA), pp 2821–2828, 10.1109/ISCAS.1992.230611.
39. Araposthatis A, Sastry S, Varaiya P (1981) Analysis of power-flow equation. *Int J Electr Power Energy Syst* 3:115–126.
40. Grijalva S, Sauer PW (2005) A necessary condition for power flow Jacobian singularity based on branch complex flows. *IEEE Trans Circ Syst I Fundam Theory Appl* 52:1406–1413.
41. Sauer PW, Lesieutre BC, Pai MA (1993) Maximum loadability and voltage stability in power systems. *Int J Electr Power Energy Syst* 15:145–153.
42. Chandrashekhar KS, Hill DJ (1986) Cutset stability criterion for power systems using a structure-preserving model. *Int J Electr Power Energy Syst* 8:146–157.
43. Gravagne IA, Walker ID (2000) On the structure of minimum effort solutions with application to kinematic redundancy resolution. *IEEE Trans Robot Autom* 16:855–863.
44. Ha I, Lee J (2002) Analysis on a minimum infinity-norm solution for kinematically redundant manipulators. *ICASE Transaction on Control Automation and Systems Engineering* 4:130–139.
45. Woods AJ, Wollenberg BF (1996) *Power Generation, Operation, and Control* (Wiley, New York), Ed 2.
46. Bürger M, Zelazo D, Allgöwer F (2012) Hierarchical clustering of dynamical networks using a saddle-point analysis. *IEEE Trans Automat Contr* 58(1):113–124.
47. Ning S, Kearfott RB (1997) A comparison of some methods for solving linear interval equations. *SIAM J Numer Anal* 34:1289–1305.
48. Brayton R, Hoffman A, Scott T (1977) A theorem on inverses of convex sets of real matrices with application to the worst case DC problem. *IEEE Trans Circ Syst* 24:409–415.
49. Dreyer A (2006) Interval analysis of linear analog circuits. *GAMM-IMACS International Symposium on Scientific Computing, Computer Arithmetic and Validated Numerics,* p 14, 10.1109/SCAN.2006.24.
50. Tempo R, Calafiore G, Dabbene F (2005) *Randomized Algorithms for Analysis and Control of Uncertain Systems* (Springer, New York, NY).
51. Calafiore GC, Dabbene F, Tempo R (2011) Research on probabilistic methods for control system design. *Automatica* 47:1279–1293.
52. Watts DJ, Strogatz SH (1998) Collective dynamics of 'small-world' networks. *Nature* 393(6684):440–442.
53. Hoeffding W (1963) Probability inequalities for sums of bounded random variables. *J Am Stat Assoc* 58:13–30.
54. Wang Z, Scaglione A, Thomas RJ (2010) Generating statistically correct random topologies for testing smart grid communication and control networks. *IEEE Transactions on Smart Grid* 1:28–39.
55. Zimmerman RD, Murillo-Sánchez CE, Gan D (2011) MATPOWER: Steady-state operations, planning, and analysis tools for power systems research and education. *IEEE Trans Power Syst* 26:12–19.
56. Grigg C, et al. (1999) The IEEE Reliability Test System—1996. A report prepared by the Reliability Test System Task Force of the Application of Probability Methods Subcommittee. *IEEE Trans Power Syst* 14:1010–1020.
57. Varaiya PP, Wu FF, Bialek JW (2011) Smart operation of smart grid: Risk-limiting dispatch. *Proc IEEE* 99:40–57.

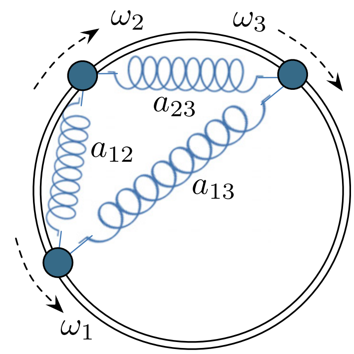

Fig. S1. Mechanical analog of the coupled oscillator model [**S1**].

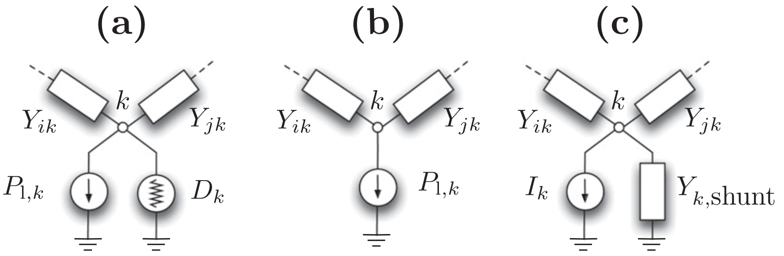

Fig. S2. Equivalent circuits of the frequency-dependent load model (*A*), the constant power load model (*B*), and the constant current and admittance load model (*C*).

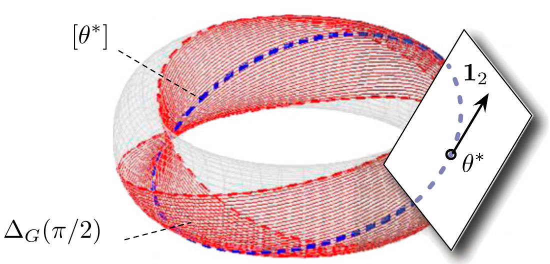

Fig. S3. Illustration of the state space $\mathbb{T}^2$, the set $\Delta_G(\pi/2)$, the synchronization manifold $[\theta^*]$ associated with a point $\theta^* = (\theta_1^*, \theta_2^*) \in \Delta_G(\pi/2)$, the tangent space at θ^*, and the translation vector $\mathbf{1}_2$.

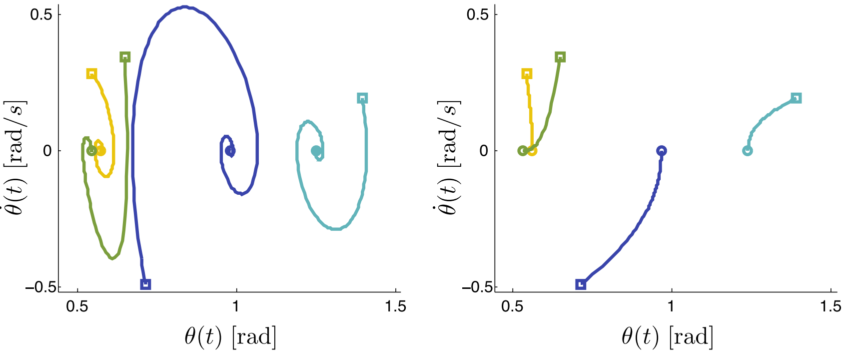

Fig. S4. (*Left*) Plot shows the phase space dynamics of a network of $n = 4$ second-order oscillators [**S3**] with $\mathcal{V}_2 = \emptyset$ and Kuramoto type coupling $a_{ij} = K/n$ for all distinct $i, j \in \mathcal{V}_1 = \{1, \ldots, 4\}$ and for $K \in \mathbb{R}$. (*Right*) Plot shows the phase space dynamics corresponding to first-order Kuramoto oscillators [**S2**], together with the frequency dynamics $\frac{d}{dt}\dot{\theta} = -M^{-1}D\dot{\theta}$. The natural frequencies ω_i and the coupling strength K are chosen such that $\omega_{\text{sync}} = 0$ and $K = 1.1 \cdot \max_{i,j \in \{1,\ldots,4\}} |\omega_i - \omega_j|$. From the same initial configuration $\theta(0)$ (denoted by □), both first- and second-order oscillators converge exponentially to the same synchronized equilibria (denoted by ○), as predicted by *Lemma 1*.

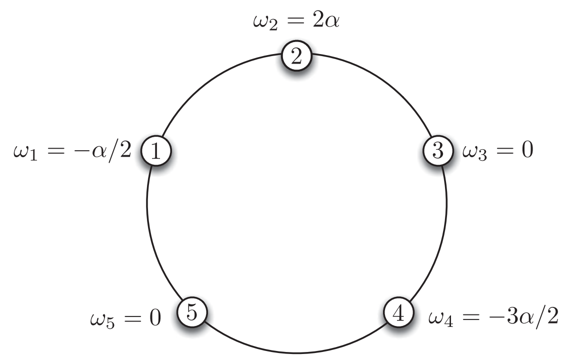

Fig. S5. Cycle graph with $n = 5$ nodes and a nonsymmetrical choice of ω.

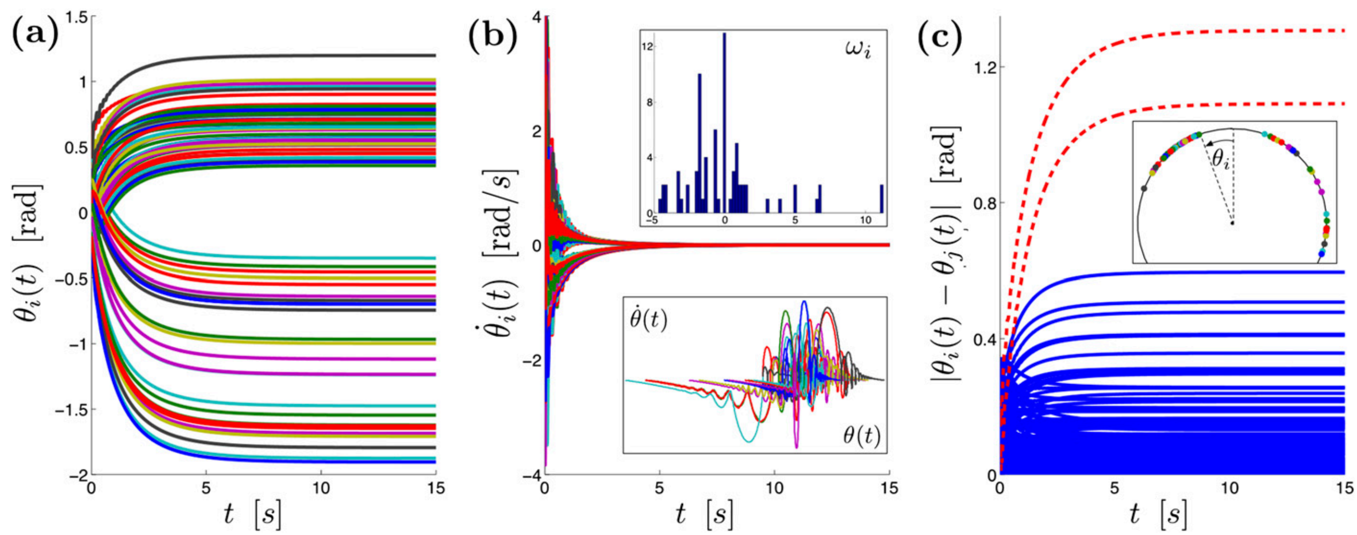

Fig. S6. Time series of the RTS 96 dynamics for a 141% load increase, resulting in $\|B^T L^{\dagger}\omega\|_{\infty} = \|L^{\dagger}\omega\|_{\mathcal{E},\infty} = 0.9995 < 1$. Angles $\theta_i(t)$ (*A*), frequencies $\dot{\theta}_i(t)$(*B*), and angular distances $|\theta_i(t) - \theta_j(t)|$ (*C*) over transmission lines are depicted, where the red dashed curves correspond to the pairs $\{121, 325\}$ and $\{223, 318\}$. (*Insets*) Power injections ω_i (*A*), the phase space of the generator dynamics $(\theta(t), \dot{\theta}(t))$ (*B*), and the stationary angles θ_i (*C*) are shown.

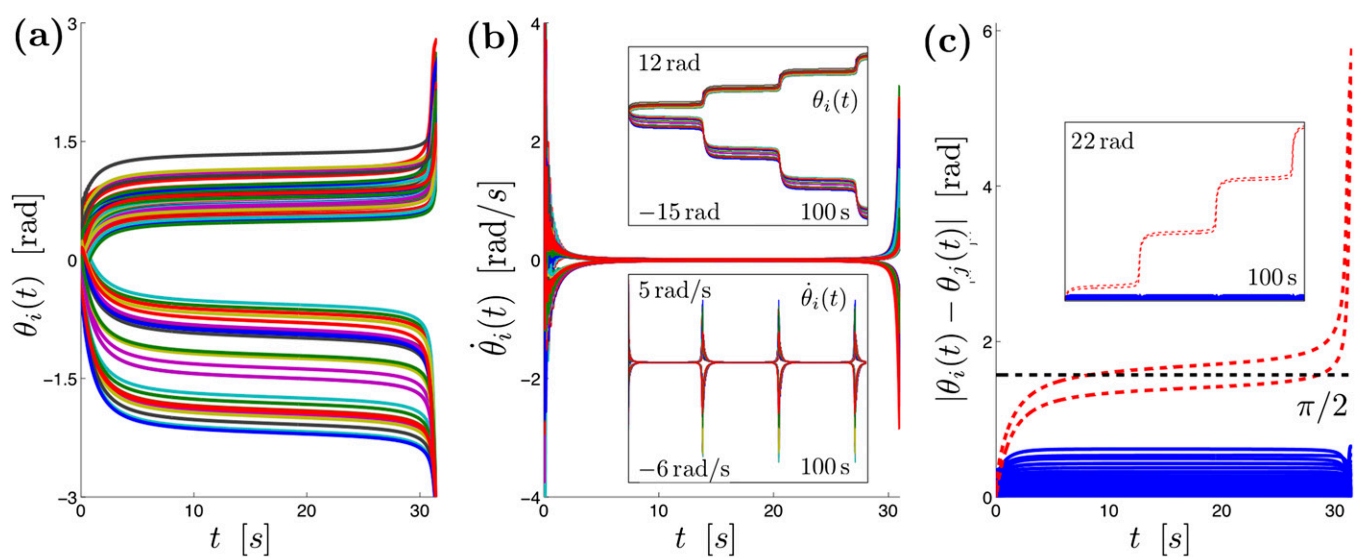

Fig. S7. Time series of the RTS 96 dynamics for a 151% load increase, resulting in $\|B^T L^{\dagger}\omega\|_{\infty} = \|L^{\dagger}\omega\|_{\mathcal{E},\infty} = 1.0560 > 1$. Angles $\theta_i(t)$ (*A*), frequencies $\dot{\theta}_i(t)$ (*B*), and angular distances $|\theta_i(t) - \theta_j(t)|$ (*C*) over transmission lines are depicted, which diverge for the pairs $\{121, 325\}$ and $\{223, 318\}$, shown as red dashed curves. (*B* and *C*, *Insets*) Long-time dynamics simulated over 100 s are shown.

Table S1. Results of the Monte Carlo simulations to test the hypothesis $\mathcal{H}$

Nominal random network parametrized by (n, RGM, p, α)	Failures of hypothesis $\mathcal{H}$: # ($\mathcal{H}$ is not true)	Empirical probability: $\widehat{\text{Prob}}_{(n,\text{RGM},p,\alpha)}$, %
(10, ERG, 0.15, 6)	104	99.653
(10, ERG, 0.3, 8)	65	99.783
(10, ERG, 0.5, 14)	15	99.950
(10, ERG, 0.75, 25)	0	100
(20 ERG, 0.15, 10)	80	99.733
(20, ERG, 0.3, 15)	5	99.983
(20, ERG, 0.5, 24)	0	100
(20, ERG, 0.75, 45)	0	100
(30, ERG, 0.15, 13)	22	99.927
(30, ERG, 0.3, 20)	0	100
(30, ERG, 0.5, 37)	0	100
(30, ERG, 0.75, 65)	0	100
(60, ERG, 0.15, 20)	1	99.997
(60, ERG, 0.3, 40)	0	100
(60, ERG, 0.5, 70)	0	100
(60, ERG, 0.75, 125)	0	100
(120, ERG, 0.15, 35)	0	100
(120, ERG, 0.3, 75)	0	100
(120, ERG, 0.5, 130)	0	100
(120, ERG, 0.75, 235)	0	100
(10, RGG, 0.3, 10)	15	99.950
(10, RGG, 0.5, 15)	18	99.940
(20, RGG, 0.3, 10)	23	99.924
(20, RGG, 0.5, 15)	3	99.990
(30, RGG, 0.3, 10)	31	99.897
(30, RGG, 0.5, 15)	1	99.997
(60, RGG, 0.3, 10)	3	99.990
(60, RGG, 0.5, 15)	0	100
(120, RGG, 0.3, 10)	0	100
(120, RGG, 0.5, 15)	0	100
(10, SMN, 0.1, 10)	2	99.994
(10, SMN, 0.2, 10)	0	100
(20, SMN, 0.1, 13)	0	100
(20, SMN, 0.2, 13)	0	100
(30, SMN, 0.1, 10)	0	100
(30, SMN, 0.2, 13)	0	100
(60, SMN, 0.1, 7)	0	100
(60, SMN, 0.2, 7)	0	100
(120, SMN, 0.1, 4)	0	100
(120, SMN, 0.2, 4)	0	100
Over all $1.2 \cdot 10^6$ instances	388	99.968

Overall, $1.2 \cdot 10^6$ instances of $\{G(\mathcal{V}, \mathcal{E}, A), \omega\}$ were constructed as described in statements (*i*)–(*iv*) in *Statistical Assessment of Correctness*, each satisfying $\|B^T L^\dagger \omega\|_\infty < 1$. For each instance, the fixed-point equation [**S7**] was solved with accuracy 10^{-6} and failures of the hypothesis $\mathcal{H}$ were reported within an accuracy of 10^{-4} (i.e., failures of order 10^{-5} were discarded).

Table S2. Evaluation of the worst-case condition [S23] for four IEEE test cases with fluctuating demand

Randomized test case (1,000 instances)	Correctness*	Accuracy†, rad	Cohesive phases‡, rad	Variations in power demand§, per unit	Variations in voltages¶, per unit
Chow 9 bus system	Always true	0.14229	0.15637	0.79891	0.19262
IEEE 14 bus system	Always true	0.20416	0.18429	1.0537	0.57177
New England 39	Always true	0.048628	0.1756	0.81972	0.077967
IEEE 118 bus system	Always true	0.097533	0.23370	0.37332	0.32301

*Correctness: $\max_{L \in \text{vert}(\mathcal{L}),\ \omega \in \text{vert}(\Omega)} \|B^T L^\dagger \omega\|_\infty \le \sin(\gamma) \Rightarrow \max_{\{i,j\} \in \mathcal{E}} |\theta_i^* - \theta_j^*| \le \gamma$.

†Accuracy: $\max_{1000\ \text{iterations}} |\max_{\{i,j\} \in \mathcal{E}} |\theta_i^* - \theta_j^*| - \arcsin(\max_{L \in \text{vert}(\mathcal{L}), \omega\ \in \text{vert}(\Omega)} \|B^T L^\dagger \omega\|_\infty)|$.

‡Phase cohesiveness: $\max_{1000\ \text{iterations}} \{\max_{\{i,j\} \in \mathcal{E}} |\theta_i^* - \theta_j^*|\}$.

§Variations in power demand: $\max_{i \in \mathcal{V}_2} \{\max_{1000\ \text{iteractions}} P_{l,i} - \max_{1000\ \text{iteractions}} P_{l,\ i}\}$.

¶Variations in load voltages: $\max_{i \in \mathcal{V}_2} \{\max_{1000\ \text{iteractions}} |V_i| - \min_{1000\ \text{iteractions}} |V_i|\}$.